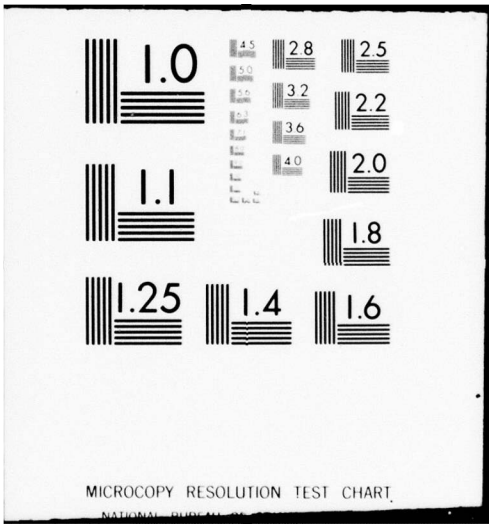
AD-A057 980 ENVIRONMENTAL RESEARCH INST OF MICHIGAN ANN ARBOR RA--ETC F/G 20/14
EFFECTS OF ATMOSPHERIC TURBULENCE ON SAR PERFORMANCE.(U)
JUN 78 G ADAMS, R CRANE, J AUTERMAN F33657-77-C-0229
UNCLASSIFIED ERIM-127800-5-F NL

1 OF 2
AD A057 980




1.0
1.1
1.25
1.4
1.6
1.8
2.0
2.2
2.5
2.8
3.2
3.6
4.0
4.5
5.0
5.6
6.3
7.1
8.0
9.0
MICROCOPY RESOLUTION TEST CHART

AD A057980

LEVEL II

(2)

127800-5-F

Final Technical Report
TEST ANALYSIS AND EVALUATION

EFFECTS OF ATMOSPHERIC TURBULENCE ON SAR PERFORMANCE

Radar and Optics Division
Environmental Research Institute of Michigan
P.O. Box 8618
Ann Arbor, Michigan 48107

JUNE 1978

AD No.
DDC FILE COPY

DDC
RECEIVED
AUG 21 1978
A

DISTRIBUTION STATEMENT A
Approved for public release;
Distribution Unlimited

Prepared for
Air Force Systems Command
Aeronautical Systems Division
Wright-Patterson AFB
Ohio 45433

78 07 07 080

UNCLASSIFIED

SECURITY CLASSIFICATION OF THIS PAGE (When Data Entered)

REPORT DOCUMENTATION PAGE	READ INSTRUCTIONS BEFORE COMPLETING FORM
1. REPORT NUMBER	2. GOVT ACCESSION NO. / 3. RECIPIENT'S CATALOG NUMBER
4. TITLE (and Subtitle): EFFECTS OF ATMOSPHERIC TURBULENCE ON SAR PERFORMANCE.	5. TYPE OF REPORT & PERIOD COVERED: Final Technical Report. February - August 1977
	6. PERFORMING ORG. REPORT NUMBER: ERIM-127800-5-F
7. AUTHOR(s): G. Adams, et al. R. Crane J. Auterman	8. CONTRACT OR GRANT NUMBER(s): F33657-77-C-0229
9. PERFORMING ORGANIZATION NAME AND ADDRESS: Radar and Optics Division, Environmental Research Institute of Michigan, P.O. Box 8618, Ann Arbor, Michigan 48107	10. PROGRAM ELEMENT, PROJECT, TASK AREA & WORK UNIT NUMBERS
11. CONTROLLING OFFICE NAME AND ADDRESS: Air Force Systems Command, Aeronautical Systems Division, Wright-Patterson AFB, Ohio 45433	12. REPORT DATE: June 1978
	13. NUMBER OF PAGES: 91 + v$_i$
14. MONITORING AGENCY NAME AND ADDRESS (if different from Controlling Office) 98p.	15. SECURITY CLASS (of this report): Unclassified
	15a. DECLASSIFICATION/DOWNGRADING SCHEDULE
16. DISTRIBUTION STATEMENT (of this Report)	
17. DISTRIBUTION STATEMENT (of the abstract entered in Block 20, if different from Report)	
18. SUPPLEMENTARY NOTES	
19. KEY WORDS (Continue on reverse side if necessary and identify by block number): Atmosphere, Turbulence, Propagation, Resolution, Synthetic Aperture Radar	

20. ABSTRACT (Continue on reverse side if necessary and identify by block number)

A study was carried out to assess the effects of atmospheric turbulence upon synthetic aperture radar (SAR) imagery. A model, based upon turbulence theory, was developed to predict the expected SAR impulse response as a function of a parameter denoted the SAR atmospheric phase error coefficient, K_ϕ. This coefficient may be calculated from measured index of refraction profiles and radar geometry. The expected SAR response was evaluated as a function of

(continued)

DD FORM 1 JAN 73 1473 EDITION OF 1 NOV 65 IS OBSOLETE

UNCLASSIFIED

SECURITY CLASSIFICATION OF THIS PAGE (When Data Entered)

78 07 07 080

408392 LB

the coefficient K_ϕ for four separate radar image processor configurations; unweighted aperture, unweighted corrected focus aperture, cosine squared weighted aperture, and 30 dB Taylor weighted aperture. Results are presented in the report.

A limited set of measurements of index of refraction profiles were made by the U.S. Department of Commerce, Office of Telecommunications. These measurements were used to calculate values of the phase error coefficient K_ϕ. These results are also presented in the report to demonstrate use of the model and to indicate the limiting effects of the atmosphere upon image quality.

The measurements indicate that atmospheric turbulence is not expected to seriously degrade the performance of currently operational systems or those operating at significantly longer ranges or finer resolutions. The measurements were limited in time, quantity, climatic conditions, and geographic locations. Extensive quantitative results will depend upon further experimental measurements.

PREFACE

This report is the final technical report for the Atmospheric Phase Error Measurements task performed under Contract F33657-77-C-0229. The work under this contract was conducted in the Radar and Optics Division of the Environmental Research Institute of Michigan (ERIM), P.O. Box 8618, Ann Arbor, Michigan. This effort was sponsored by the Air Force Systems Command, Aeronautical Systems Division, Wright-Patterson AFB, Ohio. Technical Monitors were E. Deardurff, Jr., and L. Faulkner; the Contracting Officer was H.R. Minteer, ASD/AERK. The Program Manager at ERIM was G.F. Adams.

The basic analysis was carried out by R. Crane with data calculations provided by H. Klimach, L. Wilock, and D. Franczak. R. Hamilton and T. Van Sickle assisted in documentation. The final report was written by G. Adams with major contributions from R. Crane and J. Auterman. Results of the analysis were reviewed by J. Auterman, R. Bayma, R. Heimiller, and L. Porcello.

This analysis was planned jointly with M.C. Thompson of the U.S. Department of Commerce, Office of Telecommunications. The experimental data was collected and provided to ERIM by the Department of Commerce.

ACCESSION #
NTIS White Section
DDC Buff Section
UNANNOUNCED
JUSTIFICATION
Letter on file
BY
DISTRIBUTION/AVAILABILITY CODES
Dist. AVAIL. and/or SPECIAL
A

CONTENTS

PREFACE..... iii

LIST OF FIGURES..... v

LIST OF TABLES..... vi

1. INTRODUCTION AND SUMMARY..... 1
   - 1.1 Background 1
   - 1.2 Review of Analysis 3
   - 1.3 Summary of Results 6

2. ANALYSIS..... 8
   - 2.1 Analytical Model 8
     - 2.1.1 Atmospheric Turbulence Model 9
     - 2.1.2 Synthetic Aperture Phase Model 11
     - 2.1.3 Average SAR Impulse Response 16
       - 2.1.3.1 Fixed Focus Average Response 16
       - 2.1.3.2 Corrected Focus Average Response 25
       - 2.1.3.3 Impulse Response and Phase Error Descriptors 25
   - 2.2 Experimental Data 34
     - 2.2.1 Data Collection 34
     - 2.2.2 Data Analysis 37
       - 2.2.2.1 Analytical Model Examination 37
       - 2.2.2.2 SAR Performance Analysis 55

3. CONCLUSIONS AND RECOMMENDATIONS..... 76

APPENDIX A: AVERAGE POINT TARGET RESPONSE--FIXED FOCUS..... 77

APPENDIX B: AVERAGE POINT TARGET RESPONSE--CORRECTED FOCUS..... 85

REFERENCES..... 91

FIGURES

1. SAR Geometry..... 2
2. Index of Refraction Atmospheric Model Geometry..... 10
3. SAR Atmospheric Model..... 12
4. Geometrical Models..... 14
5. Average Impulse Response for Varying Synthetic Aperture Atmospheric Phase Error Coefficient, K_ϕ..... 20
6. Rescaled Average Impulse Response Plots (Unweighted)..... 23
7. Aperture Weighted Impulse Response..... 24
8. Average Post Target Response with Focus Correction..... 26
9. Expected Impulse Response with Refocussing..... 27
10. Impulse Response Descriptors as a Function of K_ϕ..... 30
11. Typical Index of Refraction Data from Flight 6A..... 38
12. Refractive Index Constant Profiles by Flight Number and Ascent (a) or Descent (d)..... 39
13. Dependence of C_n^2 on r..... 56
14. Normalized Synthetic Aperture Phase Error Coefficient, K_{ϕ_1} for Experimental Data..... 58
15. Frequency Plots for $\delta_o K_\phi$ Vs. Range, Altitude..... 74
16. $\delta_o K_\phi$ Vs. Water Vapor Pressure..... 75

TABLES

1. Variance of Phase Error Over Aperture Versus Parameter K_ϕ 19
2. Impulse Response Descriptors 28
3. Tabulation of $ISLR_3$ Versus K_ϕ 33
4. Flight Summary 36

1
INTRODUCTION AND SUMMARY

The imaging performance of synthetic aperture radar (SAR) systems in use today does not appear to be severely limited by atmospheric propagation anomalies. Atmospheric limitation effects could become important for SAR systems operating either at longer ranges or with finer resolutions. Such systems would encounter an increase in the amount of atmosphere through which radar signals must propagate and then be coherently processed. This report describes the results of a study of these atmospheric effects. The study was performed at the Environmental Research Institute of Michigan (ERIM) and was carried out under the sponsorship of the U. S. Air Force Systems Command, Aeronautical Systems Division. It was based upon experimental atmospheric measurements collected by the U.S. Department of Commerce, Office of Telecommunications.

The study which was carried out is summarized in this first section of the report. The theory of SAR systems is briefly reviewed along with the nature of atmospheric effects, then the procedures followed during this study are described, and finally the results are summarized. The data analysis which was performed is described in detail in the second section. Conclusions and recommendations are included in the final section. Specific analytical details are included in a series of appendices.

1.1 BACKGROUND

A synthetic aperture radar (SAR) is a pulsed coherent airborne sidelooking radar system which is used to generate fine-resolution radar images of the ground. A SAR system images ground features in a two-dimensional coordinate system defined by the nominal slant range from the aircraft flight path and the distance along the flight path. The geometry of a SAR system is illustrated in Figure 1. Resolution along the slant range coordinate is achieved through the use of radar range

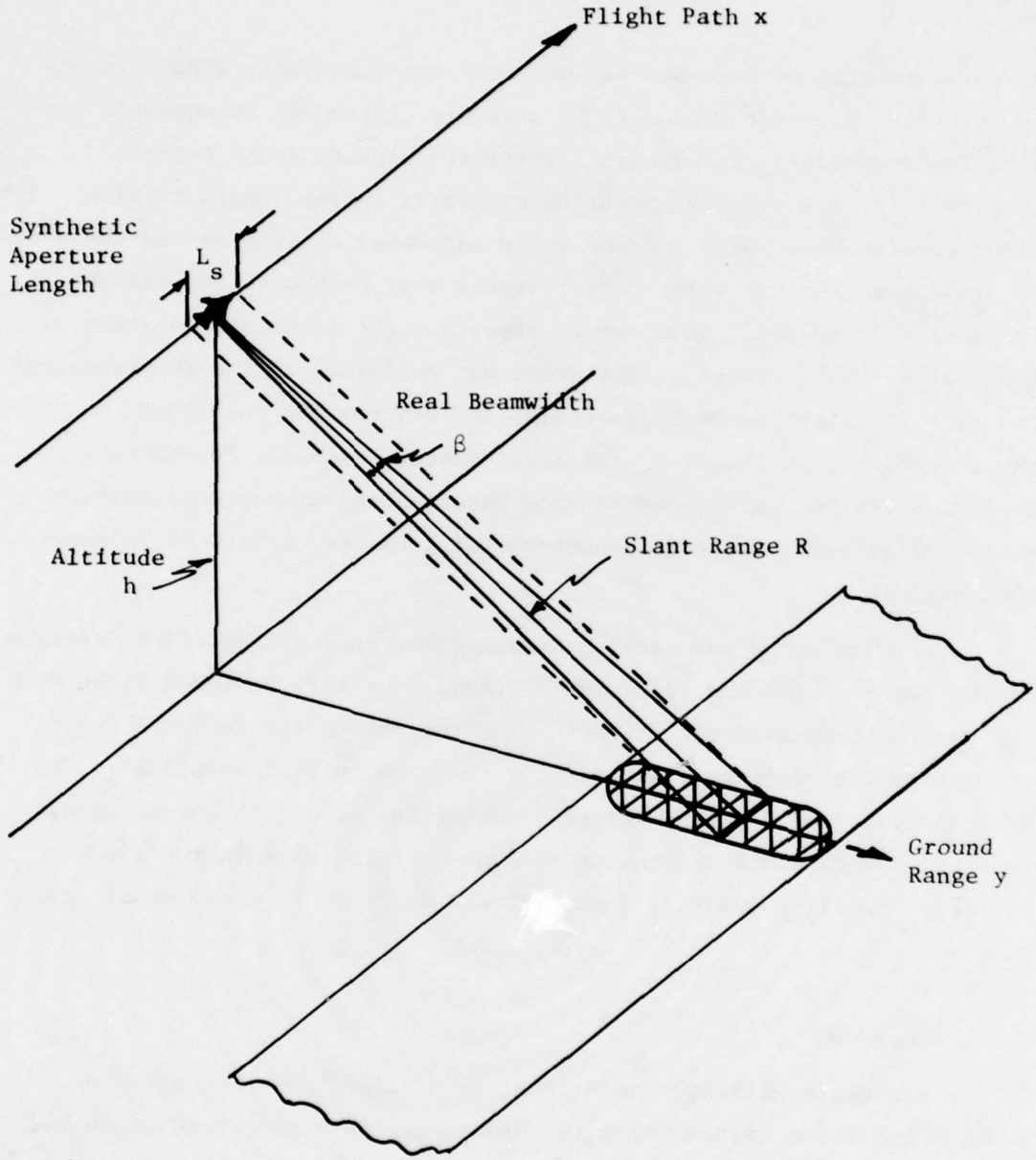


Figure 1. SAR Geometry

pulse techniques. Generally pulse compression techniques are applied using coded pulse waveforms.

Resolution in the along-track coordinate is achieved by coherently combining radar pulses received over an along-track distance called the synthetic array length. An antenna equal to this length is synthesized and the along-track resolution is determined by the synthetic array beamwidth. If data from a constant real antenna beamwidth is processed for all ranges then the synthetic array length increases linearly with range, the resultant synthetic array beamwidth decreases with range, and the theoretical synthetic along-track resolution is independent of range.

Distortion of the radar signal phase over the length of the synthetic aperture will degrade the SAR along-track impulse response performance. Therefore sources of such phase distortions and their effect upon SAR imaging performance is an important consideration in the design of such systems. These phase error sources can be divided into two general categories; those whose effect is somewhat controllable by engineering design and those over which the system designer has no control. Examples of the former include system component phase instabilities and uncorrected aircraft motion effects. Phase distortions which are caused by atmospheric propagation anomalies fall into the latter category. These types of phase errors cannot, in general, be corrected except through the use of sophisticated adaptive processing techniques. Optimum performance in the presence of propagation phase errors is an important limitation of SAR performance. It is essential that these limiting levels of performance be understood and their effects be included in system design error budgets. Thus, this study was performed to analyze the effects of such atmospheric anomaly effects.

1.2 REVIEW OF ANALYSIS

The analysis carried out during this study is briefly outlined in this section. The direct measurement of SAR signal phase errors caused by atmospheric anomalies is difficult to carry out in practice. The

problem is one of separating the effects of other phase error sources from the atmospheric propagation effects. Such phase error measurements must be made from an aircraft in order for them to be directly relatable to a SAR system. An aircraft cannot travel a perfectly straight path at a constant ground speed. Yaw, pitch, and roll variations as well as linear accelerations must be accurately determined and their phase error effects accounted for by the use of a motion compensation system. In order to measure the atmospheric phase errors, the accuracy of the motion compensation system must be such that uncompensated motion phase errors are much less than the atmospheric induced errors. This is very difficult, if not impossible, to achieve even in a carefully designed experiment. Therefore, an indirect method of determining atmospheric phase error effects upon SAR performance has been developed and was used during this study.

The indirect method used is a relatively simple method based upon the theory of radio propagation through a turbulent medium developed previously by Tatarski [1] and others. This theory was developed for the purpose of explaining variations in both the phase and amplitude of radio waves due to atmospheric index of refraction variations. Thompson, et al [2] have shown that there can be times throughout the day during which extremely large radio signal propagation amplitude variations can occur. At these times the turbulence theory cannot be directly applied. However, during the majority of time such large variations are absent and the theory can be used with a high degree of confidence. In this study, the Tatarski theory is applied to the analysis of SAR atmospherically induced phase errors. Amplitude signal variations are not considered since the phase error effects generally predominate.

---

1. Tatarski, V.I., Wave Propagation in a Turbulent Medium, Dover Publications, Inc., New York, 1961.

2. Thompson, M.C., Jr., H.B. Janes, L.E. Wood, and D. Smith, Phase and Amplitude Scintillations at 916 GHz on an Elevated Path, IEEE Trans., AP, November 1975.

The Tatarski model does not directly apply to the SAR problem. Porcello [3] earlier used the Tatarski model along with measurements by Thompson and Janes [4] to determine the statistics of the random atmospheric induced phase perturbations in SAR signals. This earlier analysis by Porcello has been extended in this report to include the simple first-order effects of a curved, rather than a flat, earth. Brown and Riordan [5] then determined the average impulse (point target) response of a SAR when phase errors caused by the atmosphere were present in the radar data.

Brown and Riordan characterized the impulse response by the use of the analytical equivalent rectangle measure of resolution. This measure corresponds directly to the reduction of the mainlobe response peak amplitude. It does not differentiate between a broadened mainlobe and increased sidelobes. During this study expected average impulse response curves were calculated and plotted for various levels of atmospheric turbulence. Then several various measures of impulse response quality were calculated for the expected impulse response curves. These include measures of mainlobe width and sidelobe levels.

A portion of the average impulse response degradation caused by atmospheric turbulence can be characterized as a simple quadratic defocusing of the radar image. The magnitude of this effect was computed and separated from the remaining higher order effects. Also, the linear portion of the phase error which causes a simple image translation was computed and separated from the phase error term.

The numerical results of this study are based upon atmospheric

---

3. Porcello, L.J., Turbulence-Induced Phase Errors in Synthetic Aperture Radars, IEEE Trans., AES, September 1970.

4. Thompson, M.C., Jr. and H.B. Janes, Measurements of Phase-Front Distortion on an Elevated Line-of-Sight Path, IEEE Trans., AES, September 1970.

5. Brown, W.M. and J.F. Riordan, Resolution Limits with Propagation Phase Errors, IEEE Trans., AES, September 1970.

index of refraction profiles measured by Thompson, et al [6]. The data collected were used to calculate values of the Tatarski model statistical propagation parameters. These values were then combined with various postulated radar configurations (ranges, altitudes, and synthetic aperture lengths) to determine numerical estimates of SAR imaging performance as limited by atmospheric effects during the days of the measurements at the measurement locations. The data used were all collected during three brief series of test flights, one over a Florida coastal region and two over a portion of Colorado. These three sets of data exhibit different results as would be expected. The results of the calculations from these measurements are included in this report.

1.3 SUMMARY OF RESULTS

The results of this study are briefly summarized in this section. A limited set of experimental atmospheric index of refraction data which was collected by Dr. M.C. Thompson of the U.S. Deparment of Commerce was analyzed during this study. The effects of atmosphere upon SAR imaging performance was determined by extending previous analyses of turbulence theory, statistical theory, and SAR theory. These results were then applied to the data collected. It should be noted here that the collected data was very limited in quantity. The data was gathered in limited geographical areas, over a limited period of time, and on a limited number of days. The capability of drawing major conclusions or extrapolating to other conditions is therefore limited.

Based on the data collected and analyzed it was shown that clear air turbulence effects would not be expected to seriously degrade the performance of the currently operational AN/UPD-4 and AN/UPD-6 SAR

---

6. Thompson, M.C., Jr., F.E. Marler, and K.C. Allen, Measurement of Refractive Index Parameters for Calculating Limits of SAR Image Resolution, OT Technical Memorandum 77-233, U.S. Department of Commerce/Office of Telecommunications, Boulder, Colorado, April 1977.

systems. Further it was shown that the performance of SAR systems operating at significantly longer ranges or finer resolutions may not be seriously limited by atmospheric effects. In fact, from the collected data only moderately degraded image quality was calculated most of the time for SAR systems operating at ranges as great as 100 nmi and impulse response widths as fine as 5 feet. On rare occasions clear air turbulence was shown to severely affect the image quality through phase error effects. It is likely that more often weather attenuation and backscatter effects as well as motion compensation effects would have seriously limited performance.

The data analysis also showed that there was no discernible relationship between ground weather measurements and the expected SAR performance during the time when the data was collected.

The data was collected during a total of 17 flights in two areas, Colorado and Florida, during the fall of 1976. Although the collected data has been extensively analyzed, there is insufficient data to begin to predict the limitations as a function of geographic location, season, time of day, or weather condition. There is insufficient data to predict expected performance variance, only the average performance was predicted for individual flights. Also, reliable measurements were not obtained in heavy rain or in heavy cloud cover and these cases are not well analyzed to date. It should be noted that measurements were gathered in an area expected to yield relatively severe effects, locally adjacent to heavy cloud cover and rain, and in light cloud cover and moderate rainstorms. It is recommended that further data collection and analysis be considered to address these limitations.

2
ANALYSIS

The goal of this analysis is to determine the extent of adverse effects on the performance of a synthetic aperture radar (SAR) due to the random phase distortions which are introduced by atmospheric propagation anomalies. The phase distortion is assumed to be caused by turbulence in the propagation medium. The analysis which was carried out is described here in two separate parts. The first part, Section 2.1, describes the theoretical model developed for the analysis which is based upon turbulence theory by Tatarski and others. The second part, Section 2.2, describes the data collection carried out by Dr. Thompson of the Department of Commerce, the analysis of the collected data, and the results of that analysis.

2.1 ANALYTICAL MODEL

The analytical model is developed in a series of three steps. The first step of this development is to determine the form of the variations in the index of refraction of the atmosphere. The atmosphere is characterized by a parameter called the atmospheric index of refraction structure function. This function describes statistically how the index of refraction varies along different paths through the atmosphere. The second step is to calculate the effect of the atmosphere upon the phase of SAR signals across the synthetic aperture. This is achieved by integrating the expected index of refraction variations along radar rays between different portions of the synthetic aperture and the ground target being imaged. A SAR phase error structure function results from this step. This structure function characterizes the expected phase variations across the synthetic aperture. The third step is then to examine the effect of this expected phase error upon SAR image quality. The expected SAR impulse response results from this step. This impulse response thus characterizes the average SAR performance as a function of atmospheric turbulence levels and system geometry.

A brief description of the details and the results of each of these analytical steps is included below. Further details are included in the appendices for those portions of the analysis which are not generally available in the referenced literature.

2.1.1 ATMOSPHERIC TURBULENCE MODEL

Tatarski [1] has analyzed the problem of radio wave phase errors caused by propagation through a turbulent medium. His analysis is based upon a term called the atmospheric index of refraction structure function. This term is used to characterize the atmosphere and is defined as

$$D_n(r) = E[n(x + r) - n(x)]^2 \tag{1}$$

The parameter n(x) is the index of refraction of the atmosphere measured along a straight path x. The operator E[ ] denotes the expected value. Thus, this structure function is the expected value of the square of the variation of the index of refraction over a distance r.

Tatarski uses physical arguments to show that for microwaves this structure function is approximately

$$D_n(r;\ h) = C_n^2(h)\ r^{2/3} \tag{2}$$

where $\ell_o << r << L_o$

where r is measured along a horizontal axis. $C_n(h)$ is the refractive index constant along a radiation path and is generally dependent only upon height h. The terms ℓ_o and L_o are called the inner and outer scales of the turbulence. The relationship shown for r and ℓ_o, L_o is generally assumed to be satisfied for the SAR cases which are analyzed herein. Figure 2 illustrates the model geometry.

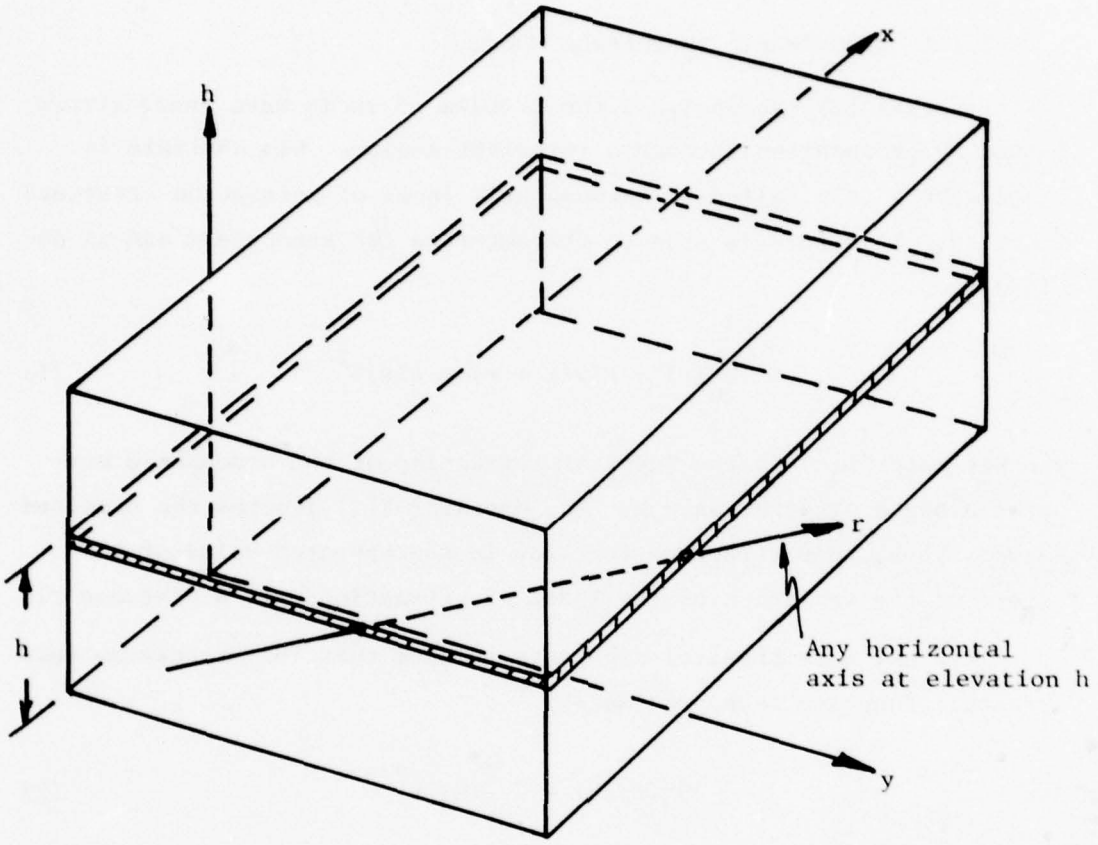


Figure 2. Index of Refraction Atmospheric Model Geometry

2.1.2 SYNTHETIC APERTURE PHASE MODEL

The structure function for the phase distribution across a synthetic aperture is defined as

$$D_{\phi}(r) = E[\phi(x + r) - \phi(x)]^2 \tag{3}$$

where x is measured along the aperture. The value of $D_{\phi}(r)$ can be found by applying the relationship

$$\phi(R) = 2k\int_0^R n(\ell)\, d\ell \tag{4}$$

where $k = 2\pi/\lambda$

R = path length.

The factor 2 must be included since the radar signal travels along the antenna to target propagation path twice, once to illuminate the target and once as reflected by the target.

The procedure followed herein is to determine the effective phase distribution across the synthetic aperture L_s as caused by the radar signal propagation through each incremental atmospheric layer. This is illustrated in Figure 3 for a layer dh thick at altitude h for a target T, slant range R, and aircraft altitude h_o. The effects of all layers will then be added together to determine the total atmospheric effect. Porcello [2] used this same approach. Strohbein [7] used a vector analysis approach and his results agreed with Porcello's results. Curtis [8], in a related study, based his analysis also upon a vector approach with similar results. He then applied a separate model for C_n which produced differing results.

---

7. Strohbein, J.W., Covariance Functions and Spectra for Waves Propagating in a Turbulent Medium to or from Moving Vehicles, IEEE Trans., AP., March 1975.

8. Curtis, D.W., Atmospheric Induced Phase Error Effects in Synthetic Aperture Radar Systems, A EEM No. 458, Goodyear Aerospace Corporation, Litchfield Park, Arizona, July 1973.

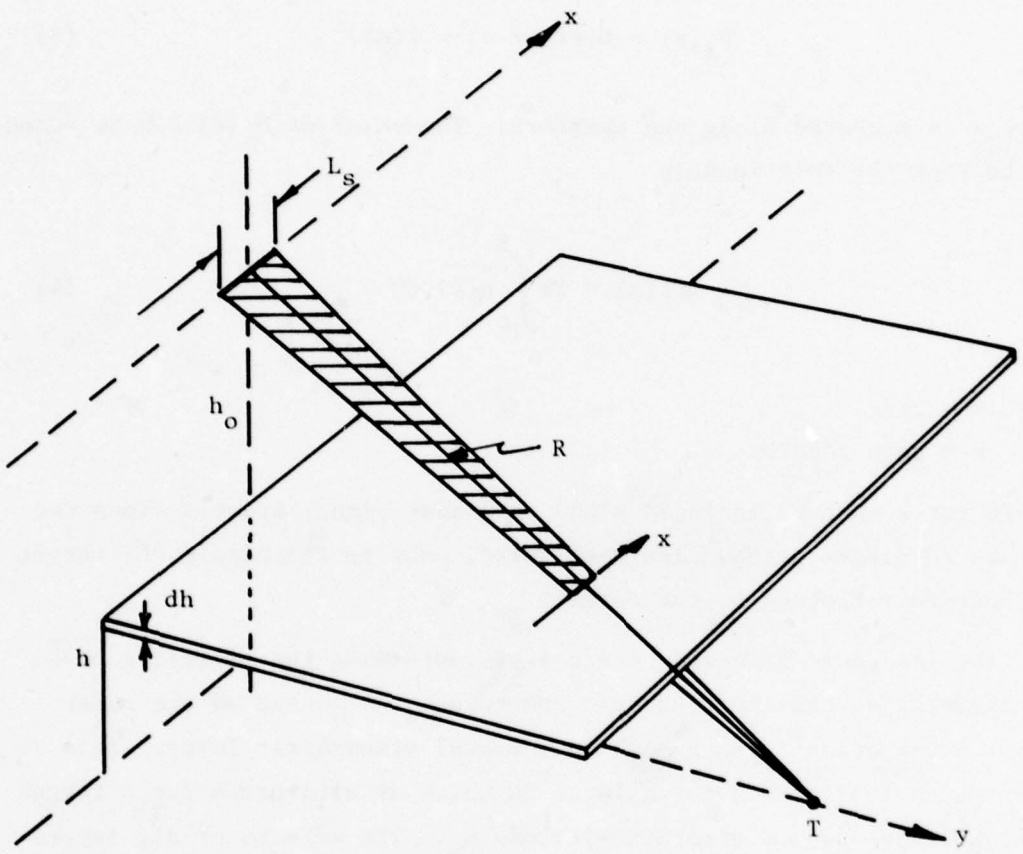


Figure 3. SAR Atmospheric Model

Tatarski, based upon his physical model results, analyzed the case for one way radio wave propagation along a path when C_n was assumed constant, such as at a constant altitude. He examined the phase array structure function $D_\phi(r)$ by evaluating the equation

$$D_\phi(r) = E\left[k\int_0^R n(\ell,x + r)\, d\ell - k\int_0^R n(\ell,x)\, d\ell\right]^2 \qquad (5)$$

The geometry of the physical model for this analysis, denoted the plane wave case, is illustrated in Figure 4(a). The calculated phase structure function is the expected value squared of the propagation path phase difference between two parallel ray paths over a total distance R as a function of path separation r. By the use of Eqs. 1 and 2 above, Tatarski found that

$$D_\phi(r) = \beta\, k^2\, R\, C_n^2\, r^{5/3} \qquad (6)$$

where $\beta = 2.91$.

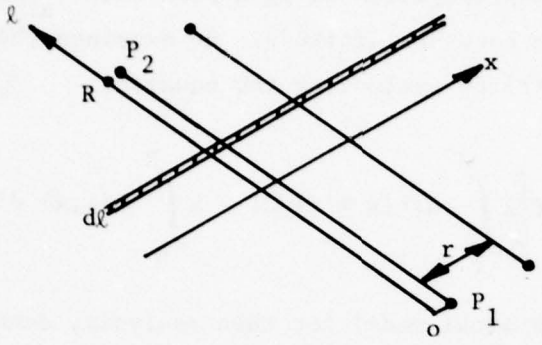
The expression for $D_\phi(r)$ can then be extended to evaluate the case when the value of C_n varies along the path. That is the case when C_n is a function of the coordinate ℓ in Figure 4(a). The incremental value of $D_\phi(n)$ due to an elemental path length $d\ell$ is

$$d\, D_\phi(r) = \beta\, k^2\, C_n^2(\ell)\, r^{5/3}\, d\ell \qquad (7)$$

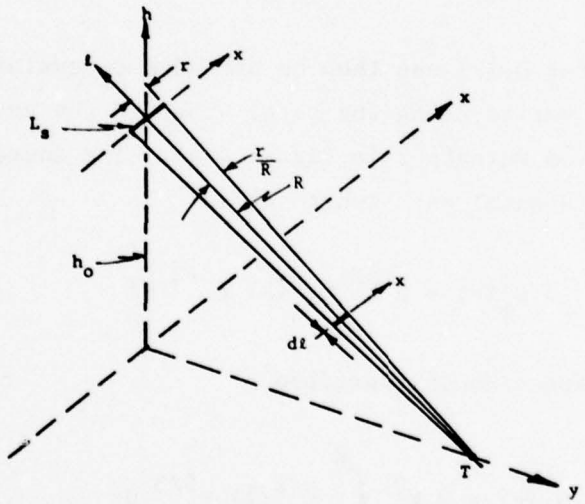
The total structure function is therefore

$$D_\phi(r) = \beta\, k^2 \int_0^R C_n^2(\ell)\, r^{5/3}\, d\ell \qquad (8)$$

This result can then, in turn, be extended to evaluate the SAR case. The SAR case, which could be called the spherical wave case, is illustrated in Figure 4(b). The various ray paths between a point being imaged (T) and the synthetic aperture (L_s) will be examined. The desired



(a) Plane Wave Model



(b) Spherical Wave Model

Figure 4. Geometrical Models

result is a structure function of the two way phase along the synthetic aperture. The incremental component of this structure function with a ray separation of $\frac{r\ell}{R}$ is

$$d\, D_\phi(r) = 4\, \beta\, k^2\, C_n^2(\ell) \left(\frac{r\ell}{R}\right)^{5/3} d\ell \qquad (9)$$

and the total structure function is

$$D_\phi(r) = 4\, \beta\, k^2 \left(\frac{r}{R}\right)^{5/3} \int_0^R C_n^2(\ell)\, \ell^{5/3}\, d\ell \qquad (10)$$

The factor four is due to the two way path factor that must be included for the radar case.

The values of C_n^2 are measured as a function of altitude h, not path distance ℓ. Therefore, a change of variables yields

$$D_\phi(r) = 4\, \beta\, k^2\, \frac{R}{h_o} \left(\frac{r}{h_o}\right)^{5/3} \int_0^{h_o} C_n^2(h)\, h^{5/3}\, dh \qquad (11)$$

or $$D_\phi(r) = C_\phi^{5/3}\, r^{5/3}$$

where $$C_\phi \triangleq \frac{1}{h_o} \left[4\, \beta\, k^2\, \frac{R}{h_o} \int_0^{h_o} C_n^2(h)\, h^{5/3}\, dh \right]^{3/5}$$

$\triangleq$ SAR Atmospheric Phase Error Constant

This relationship can be further modified to account for the first order effects of earth curvature. The resultant relationship is

$$D_\phi(r) = 4\, \beta^2\, k^2 \left(\frac{r}{R}\right)^{5/3} \int_0^{h_o} C_n^2(h)\, \frac{\left[f_e(h) - K\right]^{5/3}}{f_e(h)}\, (h + R_e)\, dh \qquad (12)$$

or $$D_\phi(r) = C_\phi^{5/3} r^{5/3}$$

where $$C_\phi \triangleq \frac{1}{R}\left[4\beta^2 K^2 \int_0^{h_o} C_n^2(h) \frac{[f_e(h) - K]^{5/3}}{f_e(h)} (h + R_e)\, dh\right]^{3/5} \qquad (13)$$

$$K \triangleq \frac{1}{2R}\left[h_o^2 + 2h_o R_e - R^2\right]$$

$$f_e(h) \triangleq \sqrt{h^2 + 2h R_e + K^2}$$

R_e = earth radius.

The relationships and models of Eqs. 12 and 13 are used as the basis of the data analysis contained in the remainder of this report.

2.1.3 AVERAGE SAR IMPULSE RESPONSE

The average or expected SAR impulse response is now determined as a function of the level of atmospheric turbulence. First, the average impulse response for normal fixed focus processing is derived assuming no other sources of phase errors. Second, the response assuming a simple focus correction is examined. Finally, in this section, the average response is characterized by various parameters such as measures of mainlobe width and sidelobe levels.

2.1.3.1 Fixed Focus Average Response

The average point target response for a SAR can be determined as a function of the phase error structure function $D_\phi(r)$ as defined in Eqs. 11 through 13. The received radar signals along the synthetic aperture due to a single target T have the form

$$s(x) = A(x)e^{j\phi(x)} e^{-j\frac{2\pi x^2}{\lambda R}} \qquad (14)$$

The amplitude term A(x) is caused by antenna pattern, radar range, and receiver characteristic effects. The random phase term $\phi(x)$ is assumed to be caused solely by the atmosphere. The remaining phase term is the geometric variation in the range to the target along the synthetic array. This is the phase term which is "matched" in order to create a radar image. Such a matched filter receiver can be modeled to have an impulse response of

$$h(x) = e^{+j \frac{2\pi x^2}{\lambda R}} \qquad |x| \leq \frac{L_s}{2} \tag{15}$$

$$= 0 \qquad \text{otherwise}$$

The receiver output magnitude is simply the magnitude of

$$f(x) = \int_{-\frac{L_s}{2}}^{\frac{L_s}{2}} A(u)\, e^{j\phi(u)}\, e^{-j \frac{4\pi xu}{\lambda R}}\, du \tag{16}$$

The amplitude term over the processing aperture L_s can be controlled to shape the nominal impulse response, especially to control sidelobe levels.

A derivation of the average point target response using results of the previous section is contained in Appendix A. The linear component of the phase error term $\phi(x)$ is removed while computing the average response since that term causes a simple point target image position shift but does not modify the image shape. The resultant phase error is then assumed to be Gaussian. Results of the derivation from Appendix I are that the expected response is

$$E|f_1(x)|^2 = L_s^2\, g_1\left(\frac{x}{\delta_o}\,;\, K_\phi\right) \tag{17}$$

The function $g_1\left(\frac{x}{\delta_o}; K_\phi\right)$ is the normalized average point target response

of the radar and δ_o is the nominal unweighted impulse response width of the radar where

$$\delta_o \triangleq \frac{\lambda R}{2L_s} \tag{18}$$

This value of δ_o is equal to half the null-to-null width of the ideal unweighted impulse response.

The parameter K_ϕ can be called the synthetic aperture phase error coefficient due to atmospheric anomalies. The value of this coefficient is the product of half the synthetic aperture length and the atmospheric phase error constant. It is defined as

$$K_\phi \triangleq \frac{L_s}{2} C_\phi \tag{19}$$

$\triangleq$ Synthetic Aperture Atmospheric Phase Error Coefficient

where C_ϕ was previously defined by Eq. 13. The value of K_ϕ is determined by the aperture size, the system geometry, and the atmospheric conditions.

The expected variations of the phase error across the synthetic aperture can be determined from Eqs. 3, 12, and 19 to be

$$D_\phi\Big|_{r=L_s} = (C_\phi r)^{5/3}\Big|_{r=L_s} = (2K_\phi)^{5/3} \tag{20}$$

If $K_\phi = 1$ then D_ϕ is equal to π radians across the aperture. Table 1 lists values of D_ϕ versus K_ϕ. The greater the turbulence, the greater the value of K_ϕ. When there is no atmospheric phase error then $K_\phi = 0$.

The normalized average response $g_1\left(\frac{x}{\delta_o} ; K_\phi\right)$ has been evaluated. The results are illustrated in Figure 5 for five separate values of K_ϕ. When there is no phase error and $K_\phi = 0$ then

TABLE 1. VARIANCE OF PHASE ERROR OVER APERTURE VERSUS PARAMETER K_ϕ

K_ϕ	D_ϕ
0	0
1	$3.17 \approx \pi$
2	$10 \approx 3.2\ \pi$
3	$19.8 \approx 6.3\ \pi$
4	$32 \approx 10\ \pi$
6.7	$76.6 \approx 24\ \pi$

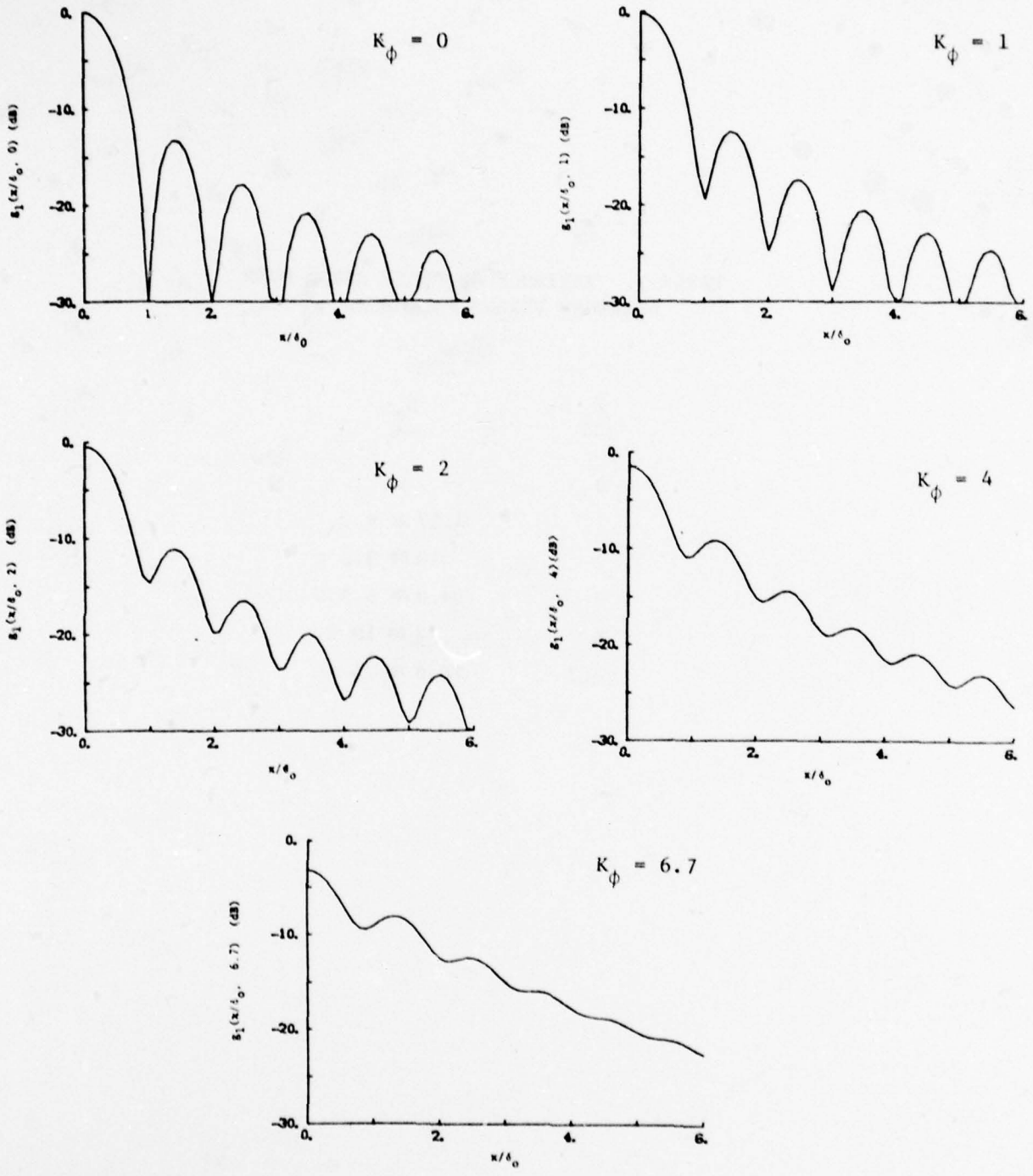


Figure 5. Average Impulse Response for Varying Synthetic Aperture Atmospheric Phase Error Coefficient, K_ϕ

$$g_1\left(\frac{x}{\delta_o}\right) = \left(\frac{\sin \pi\, x/\delta_o}{\pi\, x/\delta_o}\right)^2 \qquad (21)$$

This function has been normalized so that the peak value is unity and the first nulls occur at $x = \pm 1$. Note from Figure 5 that as the phase error coefficient increases the peak value decreases, the nulls begin to fill in, and the sidelobe levels increase.

The phase error coefficient is determined by both the synthetic aperture size and the atmospheric phase error constant. Thus the phase error coefficient can increase with either the aperture size or atmospheric turbulence. The coordinate x is normalized by the aperture size. In other words, for a fixed aperture the curves may be compared directly to illustrate the effect of varying atmospheric phase errors while for a varying aperture with fixed turbulence the coordinate x as well as the phase error coefficient must be varied. These general normalized curves can be used to illustrate any combination of these cases but they must be carefully interpreted.

The curves of Figure 5 have been redrawn in Figure 6 to illustrate various types of comparisons which could be made. In Figure 6(a) the normalized curves of Figure 5 have been simply superimposed to illustrate the effects of varying levels of turbulence with a fixed aperture size. Note that as the turbulence increases with a fixed aperture two major effects are evident. First, the peak response decreases and second, the sidelobe levels increase. The total energy in the response stays constant.

The curves are redrawn in Figure 6(b) with each peak value set to unity so that the detailed structure can be compared.

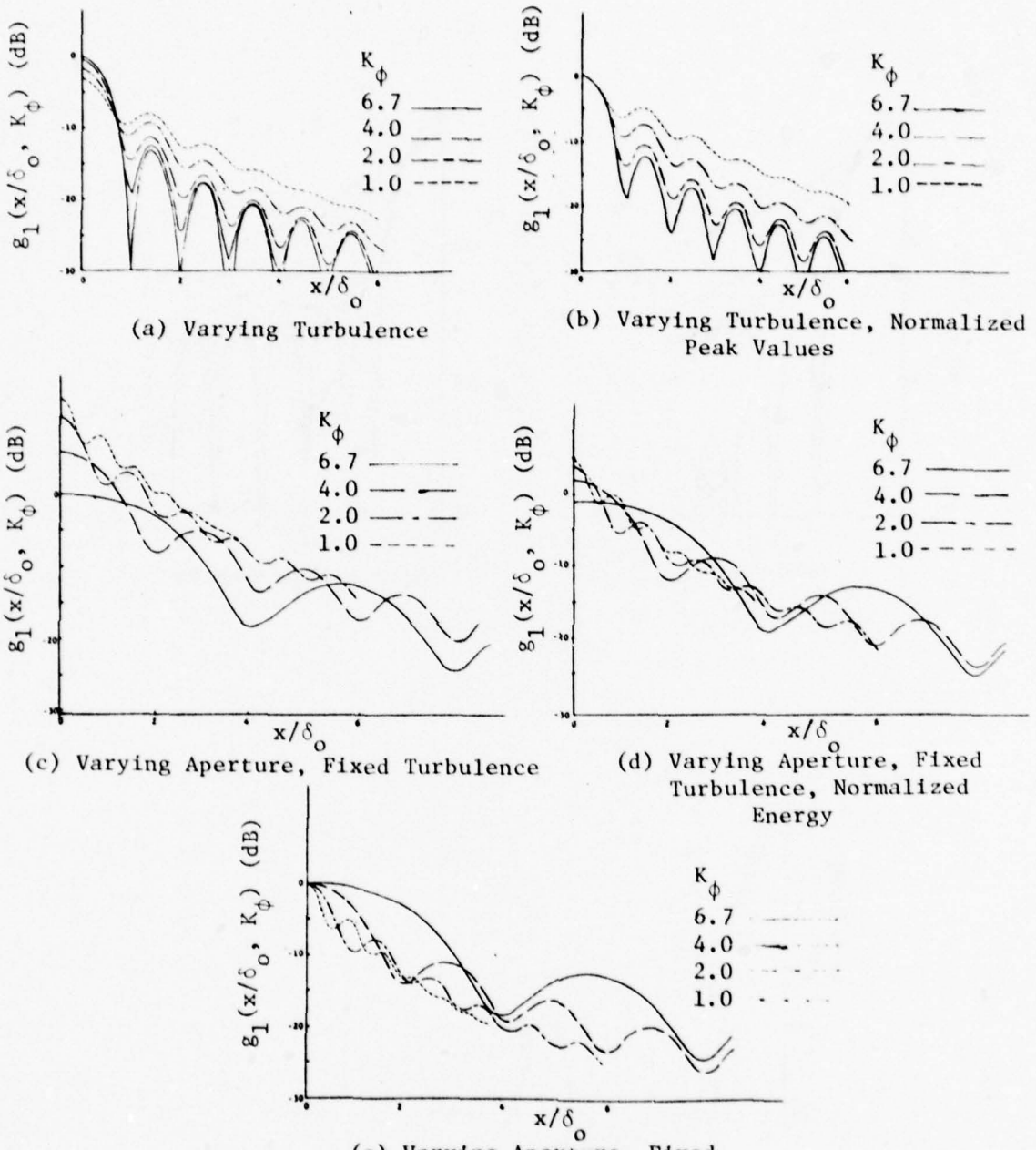
The curves in Figure 6(c), (d), and (e) show the data redrawn to compare the effect of varying the aperture size with a fixed amount of atmospheric turbulence. In Figure 6(c) the curves are drawn to show this total effect. As the aperture is made larger, the impulse response width narrows, the sidelobe levels increase with respect to the peak

value,, and both the total energy and the peak value increases. These curves are redrawn in Figure 6(d) with the amplitude normalized for constant impulse response energy. They are also redrawn in Figure 6(e) for each peak value set at unity. It can be shown that the minimum 3 dB width, maximum peak value is obtained for a value of $K_\phi = 6.7$

These curves illustrate that the choice of an optimum processing aperture must be carefully considered for each application. Many times the processing aperture is set to yield a response close to diffraction limited, i.e., with well defined nulls and first sidelobe levels close to -12 dB. This response is generally thought to be an optimum image. The choice of an optimum image under these conditions is actually a complicated one and depends upon other system parameters, such as is the system power limited or signal-to-clutter limited?

Sidelobe weighting can be used to control the impulse response sidelobe levels which are caused by the processing aperture function. The expected impulse response must be recalculated for such cases. This has been done for two aperture weightings, one a $\cos^2 x$ and the other a 30 dB Taylor weighting. The results of these calculations are illustrated in Figure 7. These results clearly show the effects of the phase errors for smaller values of K_ϕ when the aperture function sidelobes are reduced. If a weighting is used to achieve low sidelobes then much less phase error can be tolerated than for the unweighted aperture case. Note that the value of K_ϕ for these cases was calculated for δ as defined previously. In the weighted cases shown the nominal mainlobe width is broadened by factors of 1.8 and 1.5 respectively.

In summary, if the refractive index constant $C_n(h)$ profile is measured then the SAR atmospheric phase error constant C_ϕ can be calculated for any system aircraft altitude and target range by using Eq. 13. The phase error coefficient K_ϕ can then be determined by the processed aperture size and C_ϕ. From the parameter K_ϕ and the aperture size the average response is then known.



(a) Varying Turbulence

(b) Varying Turbulence, Normalized Peak Values

(c) Varying Aperture, Fixed Turbulence

(d) Varying Aperture, Fixed Turbulence, Normalized Energy

(e) Varying Aperture, Fixed Turbulence, Normalized Peak Values

Figure 6. Rescaled Average Impulse Response Plots (Unweighted)

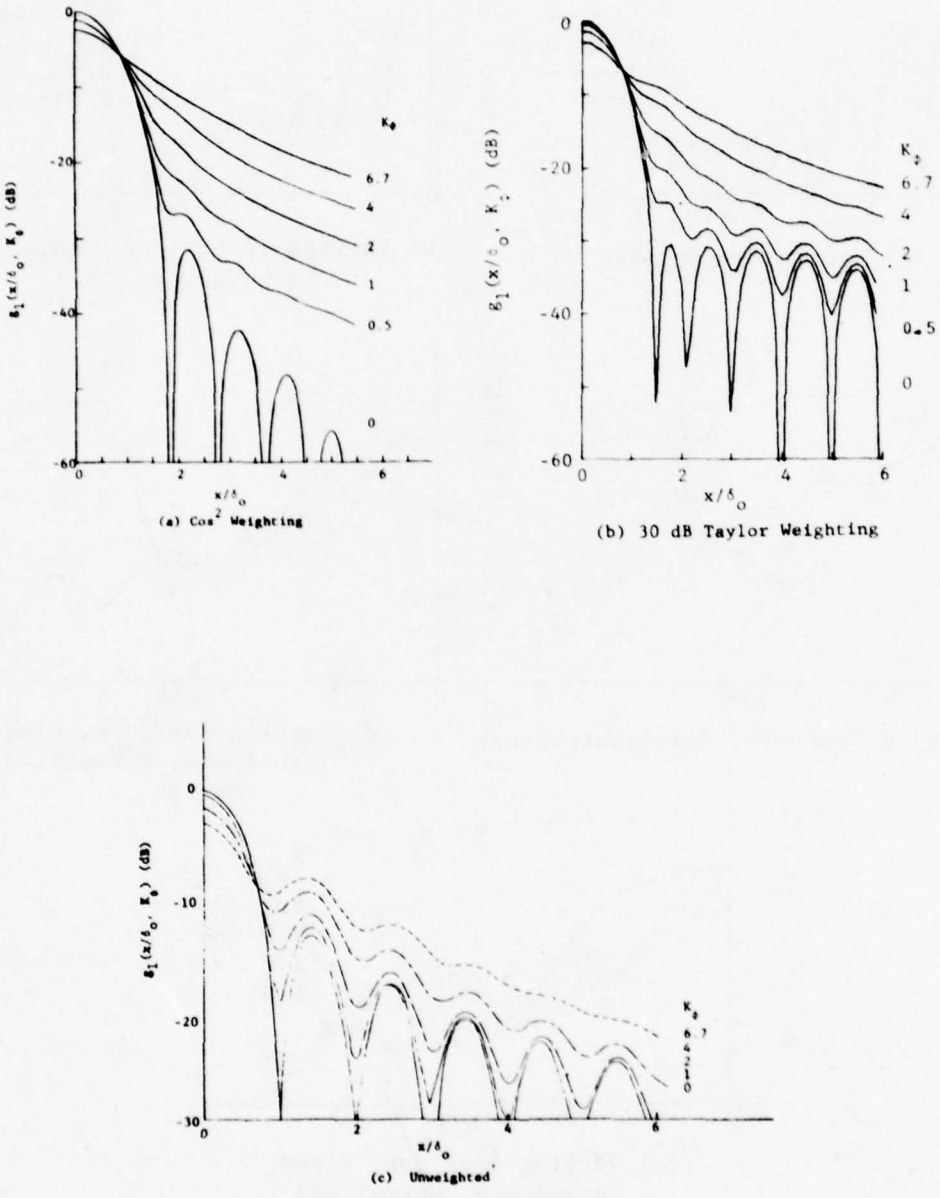


Figure 7. Aperture Weighted Impulse Response

2.1.3.2 Corrected Focus Average Response

In the analyses summarized in Section 2.1.3.1 and Appendix A both the average value and the linear component of the phase error across the synthetic aperture were ignored since they do not affect the point target impulse response shape. A third component of the phase error is the quadratic component which causes a change in target focus. This component possibly can be removed by an automatic focusing processor. A derivation of the average point target response with the quadratic term removed is contained in Appendix B. It is shown that

$$E|F_2(x)|^2 = L_s^2 \, g_2\left(\frac{x}{\delta_o} \; ; \; K_\phi\right) \tag{22}$$

The normalized refocused response $g_2\left(\frac{x}{\delta_o} \; ; \; K_\phi\right)$ has been calculated for various values of K_ϕ and is illustrated in Figure 8.

The amount of focus correction or total quadratic phase error over the processor aperture may be found from Eq. B-12 of the Appendix to be

$$\left(\frac{L_s}{2}\right)^2 \sigma_{m_2} = \left(\frac{L_s}{2}\right)^2 \left[E(m_2^2)\right]^{1/2} \cong .56 \, K_\phi^{5/6} \tag{23}$$

This total quadratic error becomes roughly 1 radian for a value of $K_\phi = 2$.

If the curves of Figures 5 and 8 are compared it is seen that the results are very similar. The amount of focus correction is not great. The focused curves exhibit a higher peak value and a narrower width mainlobe with lower near-in sidelobe levels. The two cases, both focused and unfocused, are illustrated in Figure 9 for the case of $K_\phi = 4$.

2.1.3.3 Impulse Response and Phase Error Descriptors

The average impulse response pattern shape depends upon the level

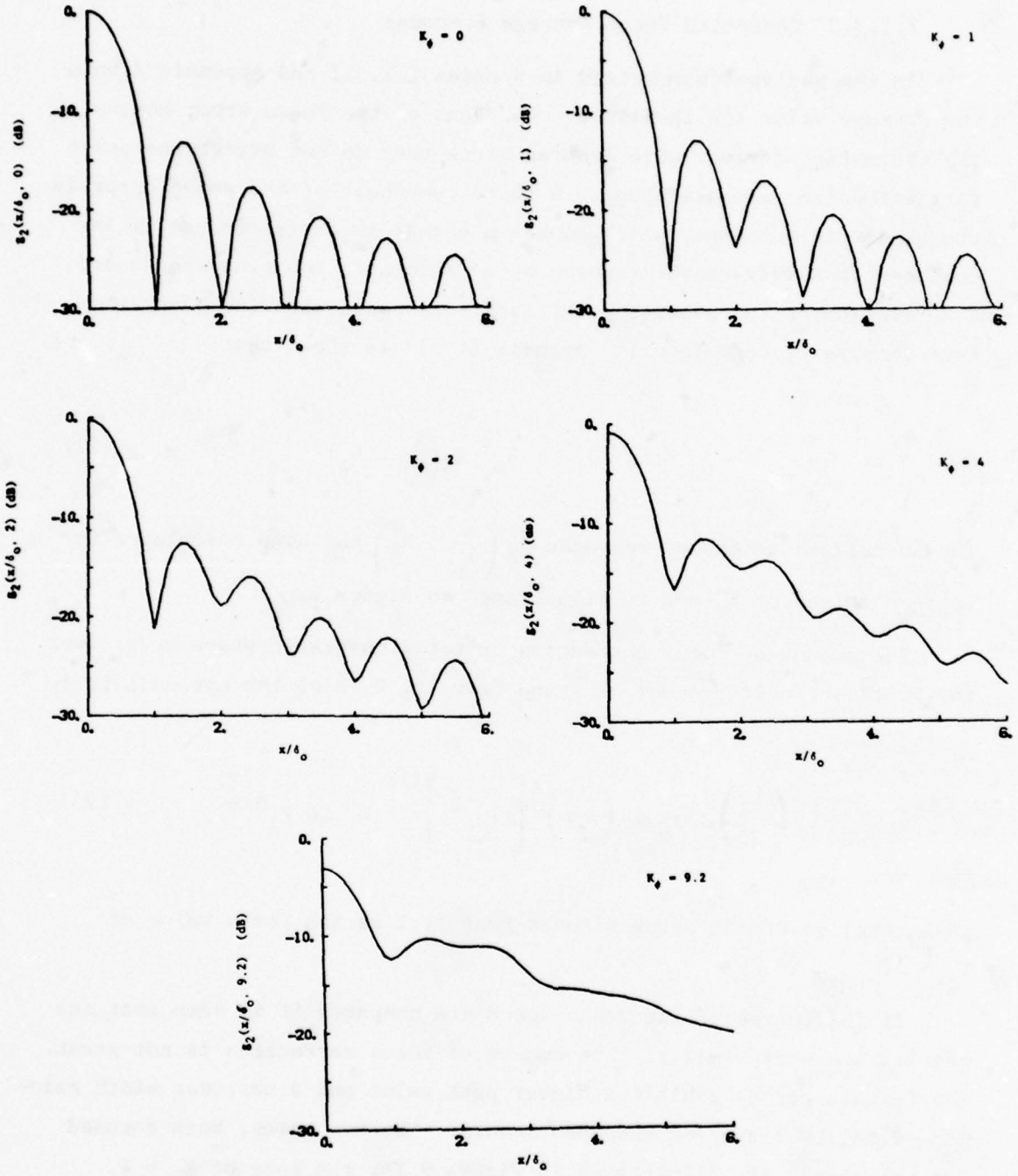
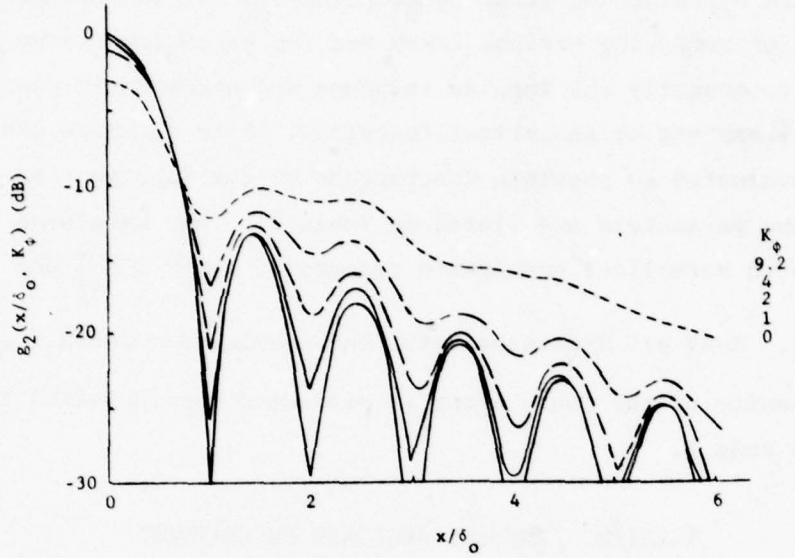
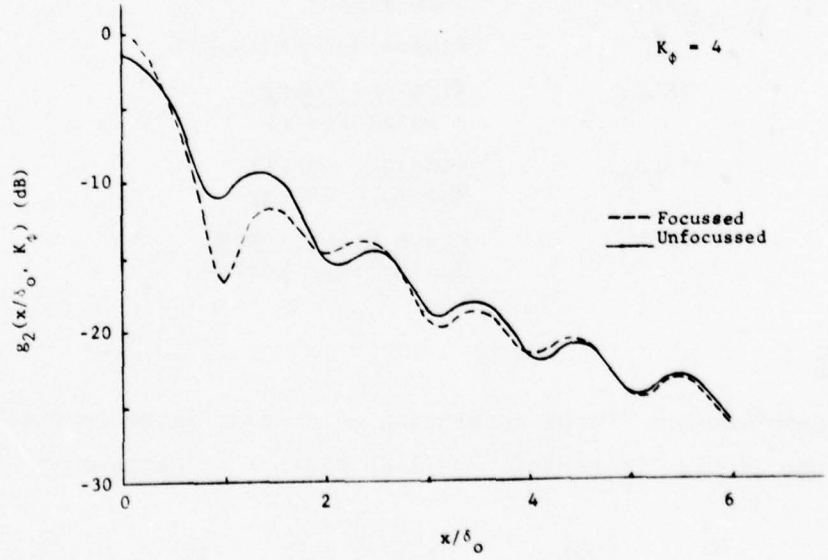


Figure 8. Average Point Target Response with Focus Correction



(a) Impulse Response, Refocussed



(b) Effect of Refocussing

Figure 9. Expected Impulse Response with Refocussing

of atmospheric turbulence, the synthetic aperture size, and the aircraft altitude and target range. As shown in the previous section the shape is determined by the phase error coefficient K_ϕ. It is desirable for the purpose of comparing various cases and for preparing system designs to be able to quantify the impulse response and atmospheric phase error by simple parameters or analytical functions. Five separate parameters have been evaluated as possible descriptors of the impulse response shape. These parameters are listed in Table 2. They have been calculated for both normalized unweighted responses, $g_1\left(\frac{x}{\delta_o} ; K_\phi\right)$ and $g_2\left(\frac{x}{\delta_o} ; K_\phi\right)$. They are discussed below and results are shown. Also, the spectral density of the phase error is presented for inclusion into a phase error budget.

TABLE 2. IMPULSE RESPONSE DESCRIPTORS

Symbol	Description
W	3 dB Width
μ	Equivalent Rectangle
$ISLR_1$	$\frac{\text{Sidelobe Energy}}{\text{Total Energy}}$
$ISLR_2$	$\frac{\text{Sidelobe Energy}}{\text{Mainlobe Energy}}$
$ISLR_3$	$\frac{\text{Phase Error Energy}}{\text{Undistorted Energy}}$

3 dB Width

A common measure of the resolution of a radar image is the 3 dB width of the impulse response. The 3 dB width W is defined by

$$g\left(\frac{2L_s}{\lambda R}\ \frac{W}{2} ; K_\phi\right) = \frac{1}{2}\, g\left(0 ; K_\phi\right) \qquad (24)$$

The value of W has been calculated as a function of the phase error

coefficient K_ϕ and is illustrated in Figure 10. Note that the 3 dB width increases slightly with K_ϕ. This measure of impulse response quality is nearly exclusively determined by the processing aperture size, not by the level of phase error.

Equivalent Rectangle

The equivalent rectangle μ is defined as the width of a rectangle whose height is equal to the average response peak value and whose energy is the same as the average response energy. This definition can be expressed as

$$\mu = \frac{\int_{-\infty}^{\infty} |g(x/\delta_o ; K_\phi)|^2 \, dx}{|g(0 ; K_\phi)|} \tag{25}$$

which becomes

$$\mu = \frac{R\lambda}{2L_s} \frac{1}{g(0 ; K_\phi)} \tag{26}$$

If there are no atmospheric phase errors then μ equals $\frac{\lambda R}{2L_s}$. The value of μ is simply a measure of the peak value of the average response and therefore is not a very useful direct measure of image quality. The dependence of μ on K_ϕ is shown in Figure 10. For the case analyzed in this study the decrease in peak value, or increase in μ, is most directly related to the increase in impulse response sidelobe levels. Therefore, the parameter μ is more nearly a measure of sidelobe levels rather than mainlobe width.

$ISLR_1$

One measure of integrated sidelobe energy, $ISLR_1$, is defined as the sidelobe energy of the normalized impulse response divided by the total response energy. For this purpose the separation point between

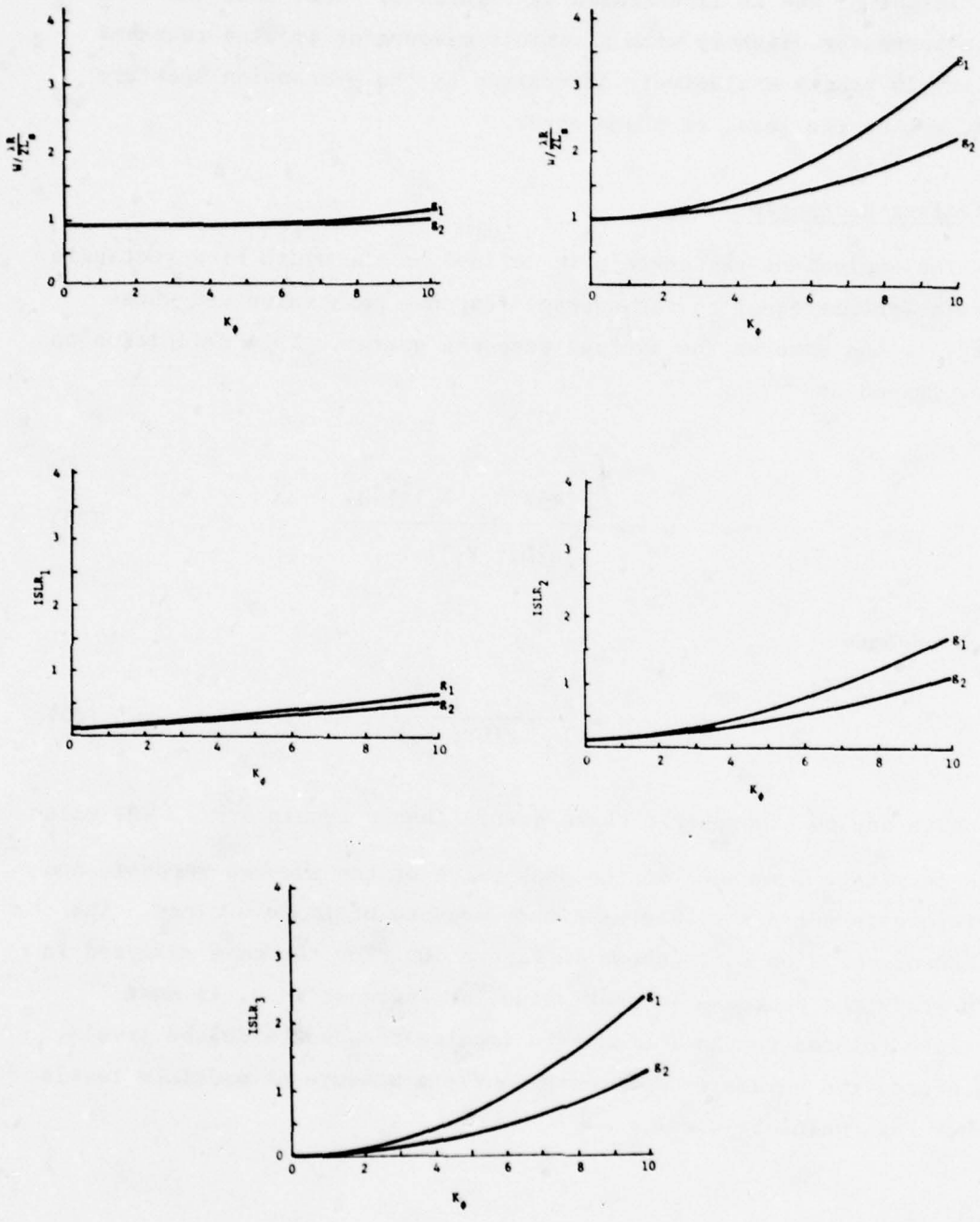


Figure 10. Impulse Response Descriptors as a Function of K_ϕ

the mainlobe and sidelobe is defined as the point where the first zero would occur in the pattern if there were no phase errors. $ISLR_1$ can be written

$$ISLR_1 = \int_{-\infty}^{-1} g(x;K_\phi)\, dx + \int_{+1}^{\infty} g(x;K_\phi)\, dx$$
$$= 1 - \int_{-1}^{1} g(x;K_\phi)\, dx \qquad (27)$$

The dependence of $ISLR_1$ on K_ϕ is also shown in Figure 10.

$\underline{ISLR_2}$

A closely related measure of sidelobe energy, $ISLR_2$, is the ratio of sidelobe to mainlobe energy. It can be written as

$$ISLR_2 = \frac{\int_{-\infty}^{-1} g(x;K_\phi)\, dx + \int_{+1}^{\infty} g(x;K_\phi)\, dx}{\int_{-1}^{+1} g(x;K_\phi)\, dx}$$
$$= \frac{ISLR_1}{1 - ISLR_1} \qquad (28)$$

This is also illustrated in Figure 10.

$\underline{ISLR_3}$

A third measure of sidelobe energy, $ISLR_3$, is the energy contained in the impulse response due to the distorted phase divided by the energy due to the undistorted phase. This definition was used by Curtis. When the phase errors are small we can assume that

$$e^{j\phi(x)} \cong 1 + j\phi(x) \tag{29}$$

The impulse response from Eq. 16 is

$$F(x) = \int_{\frac{-L_s}{2}}^{\frac{L_s}{2}} A(u)\ [1 + j\phi(u)]\ e^{-j\frac{4\pi xu}{\lambda R}}\ du \tag{30}$$

The total response energy for A(u) = 1 is

$$\int_{-\infty}^{\infty} |F(x)|^2\ dx = \frac{R\lambda}{2}\left[L_s + \int_{\frac{-L_s}{2}}^{\frac{L_s}{2}} |\phi(u)|^2\ du\right] \tag{31}$$

Therefore

$$ISLR_3 = \frac{1}{L_s}\int_{\frac{-L_s}{2}}^{\frac{L_s}{2}} |\phi(u)|^2\ du \tag{32}$$

This has been evaluated and is also shown in Figure 10. Table 3 listing values for $ISLR_3$ has been prepared since the curves cannot be easily read for small values of K_ϕ.

Spectral Density

The spectral density of the total phase error function is an important parameter to a system designer. Equations 3 and 13 showed that

$$\begin{aligned} D_\phi(r) &= C_\phi^{5/3}\ r^{5/3} \\ &= E[\phi(x + r) - \phi(x)]^2 \end{aligned} \tag{33}$$

TABLE 3. TABULATION OF $ISLR_3$ VERSUS K_ϕ

	$ISLR_3$ (dB)	
K_ϕ	g_1	g_2
0.1	-31.0	-33.0
0.2	-25.9	-28.5
0.3	-22.9	-25.5
0.4	-20.8	-23.4
0.5	-19.2	-21.8
0.6	-17.9	-20.5
0.7	-16.7	-19.4
0.8	-15.8	-18.4
0.9	-14.9	-17.5
1.0	-14.1	-16.8
1.2	-12.8	-15.4
1.4	-11.7	-14.3
1.6	-10.7	-13.3
1.8	- 9.8	-12.5
2.0	- 9.0	-11.7
2.5	- 7.4	-10.0
3.0	- 6.0	- 8.7
3.5	- 4.8	- 7.5
4.0	- 3.8	- 6.5

It can be shown that the spectral density of this phase error along the aperture is

$$S(\omega) = \frac{1}{2}\,\Gamma\left(\frac{8}{3}\right)\, C_{\phi}^{5/3}\, |\omega|^{-8/3} \qquad (34)$$

2.2 EXPERIMENTAL DATA

Experimental measurements of the atmospheric index of refraction were made by the U.S. Department of Commerce. The data collected were reduced into profiles of the refractive index constant $C_n(h)$. These results were then provided to ERIM for analysis of the expected SAR performance as a function of geometric radar parameters based upon the model described in Section 2.1. The results of this data collection and analysis are described in this section. In Section 2.2.1 the data collection phase is briefly reviewed. In Section 2.2.2 the data analysis results are presented.

2.2.1 DATA COLLECTION

A separate experimental aircraft flight test program was carried out by the U.S. Department of Commerce, Office of Telecommunications. The purpose of this flight test program was to make measurements of index of refraction profiles to be used in this analysis of the effect of atmospheric variations upon synthetic aperture radar performance. The data collected was reduced into profiles of the index of refraction constant C_n^2 and was then supplied to ERIM for the application to SAR performance estimates. The data collected and supplied to ERIM are presented in detail in a separate report [6] published by the U.S. Department of Commerce and are only briefly presented herein.

The data collection was based upon measurement techniques and equipment which have been developed over a period of several years at the U.S. Department of Commerce [9]. The instrumentation package is

---

9. Vetter, M.J. and M.C. Thompson, Jr., Solid-State Microwave Refractometer, Rev. Sci. Instrum., Vol. 38, No. 12, 1967, pp. 1726-1727.

relatively small (total weight 33 pounds) and can be rapidly installed and used on a wide variety of small aircraft. The major component of the equipment is an ITS model 6 X-band refractometer which provides analog measurements of the atmospheric index of refraction, temperature, and pressure. In the current system these measurements are filtered, digitized, and recorded on magnetic tape for subsequent analysis. The data collection system was modified specifically for this program to provide an increased spatial data sampling rate.

During this program, three sets of data gathering flights were flown for a total of 17 separate flights. The initial set of five flights were flown in an area near the Boulder, Colorado, U.S. Department of Commerce laboratory. These initial flights were carried out for the purpose of testing and calibrating the modified instrumentation package and to provide a sample data base. The second set of nine flights were flown in an area close to Eglin Air Force Base, Florida. The purpose of these flights were to gather data, for the analysis, which would exhibit samples from relatively severe atmospheric conditions. The Eglin area was chosen due to its close proximity to a land/water boundary and due to the prevailing local weather (temperature/humidity) conditions. A third set of three additional flights were flown near the Boulder laboratory. The purpose of these final flights was to provide additional data up to higher altitudes during a different season of the year. The total amount of data gathered were severely limited in terms of numbers of flights, seasonal, diurnal, and geographic considerations but were deemed sufficient to provide significant results from the subsequent analysis.

Two different types of flight paths were flown. One type used was composed of a series of level runs at 1,000 ft altitude intervals. The other type was a steady and shallow, spiral or straight, ascent or descent. The specific flights carried out are summarized in Table 4. Flights were flown to altitudes as high as 29,000 ft. Data were gathered under a variety of weather conditions although all flight patterns were chosen so that VFR conditions were maintained. Data were

TABLE 4. FLIGHT SUMMARY

FLT. NO.	DATE/TIME		LOCATION	MAX.ALT. K-Ft.	TYPE REMARKS
1	8/30/76	1000/1130	Colorado	9.5	Ladder ascent with level runs; constant descent on E, W course from Longmont
2	9/3/76	1300/1500	"	12.5	" " " " " " "
3	9/21/76	0830/1130	"	12.5	" " " " " " "
4	9/28/76	1230/1410	"	11.5	Slant ascent from Longmont towards Jackson Reservoir; ladder descent with level runs on NE, SW course from Jackson Reservoir
5	9/29/76	1230/1530	"	12.5	" " " " " " "
6	10/8/76	1600/1830	Florida	20.5	Spiral ascent, ladder descent from Panama City towards Dothan, ALA.
7	10/11/76	0930/1230	"	23.0	Spiral ascent, ladder descent takeoff Dothan, ALA, spiral up east of airport.
8	10/12/76	0840/1050	"	23.3	Spiral ascent, ladder descent over coastline ~ 10 mi. S of Tyndall AFB
9	10/13/76	2100/2400	"	23.6	Slant ascent east and descent west, Panama City to Jacksonville
10	10/14/76	1330/1630	"	24.0	Slant ascent and descent over Gulf on 190° radial from Panama City
11	10/15/76	1000/1400	"	25.0	Slant ascent east to Jacksonville, descent west to Panama City
12	10/16/76	1030/1340	"	25.0	Slant ascent SE towards Tampa, descent NW to Panama City, FLA, following the coastline on both ascent and descent.
13	10/18/76	1100/1400	"	25.0	Slant ascent and descent over Gulf on 185° radial from Panama City, FLA
14	10/19/76	1000/1300	"	24.0	Slant ascent toward west to Gulfport, MISS, descent east to Panama City, FLA, following coastline on both ascent and descent.
15	11/16/76	1430/1700	Colorado	28.5	Ascent and descent "figure 8" vertical, and Longmont, CO, as turning points
16	11/17/76	1230/1530	"	28.0	Slant ascent toward north from Boulder, descent south toward Boulder
17	11/19/76	0900/1230	"	29.0	Slant ascent toward east from Boulder, descent west toward Boulder

gathered during rain and on a few occasions raindrops caused abnormal refractivity readings so that data collected at these times were ignored.

The measured index of refraction (n) data were used to calculate index of refraction structure function (C_n^2) profiles. Figure 11 illustrates examples of typical measured index of refraction data. The data were measured such that independent samples were obtained at a spatial rate of roughly one per meter. Each of the C_n^2 profiles, along with temperature and refractivity profiles are presented in the U.S. Department of Commerce report. The C_n^2 profiles are reproduced in Figure 12. The values of $C_n^2(h)$ were computed at 1,000 ft altitude intervals for each data set except sets 5-D, 6-D, and 7-D where 500 ft intervals were used.

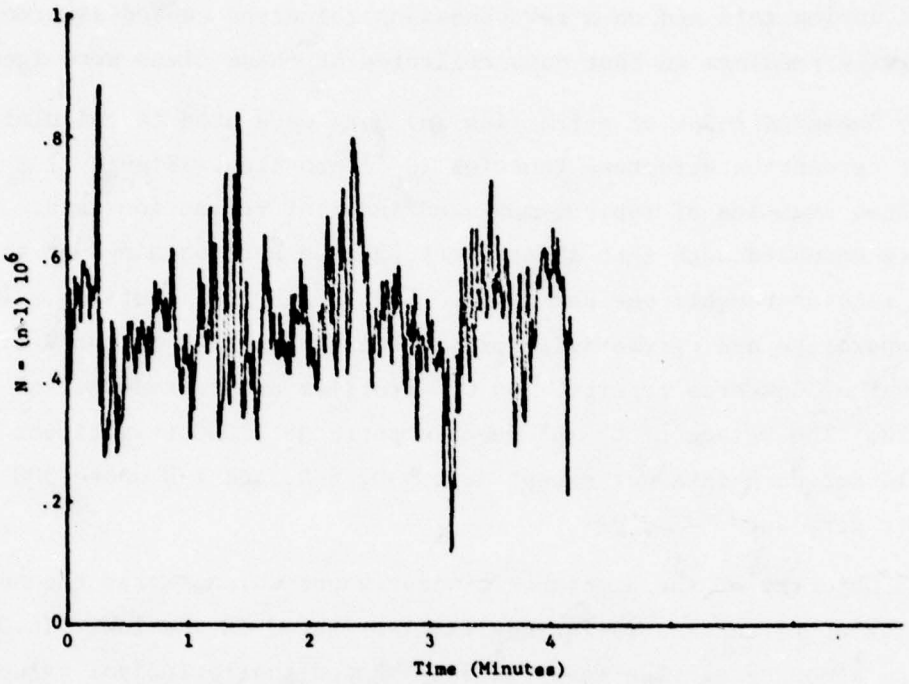
The majority of the atmospheric water vapor which causes the subject index of refraction variations is distributed in the lower 15,000 ft of the atmosphere. The measured data showed that principal values of C_n^2 were below the 10,000 ft altitude. In a few cases, there were significant values up to 20,000 ft but in all of these cases this amounted to a fraction of the peak value.

2.2.2 DATA ANALYSIS

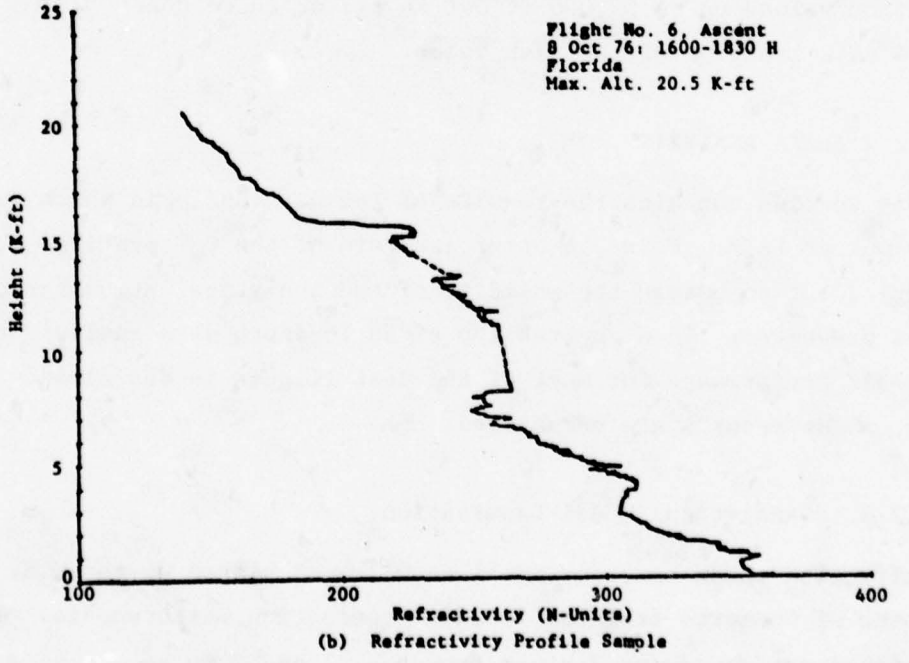
This section contains the results of the data analysis which was carried out at ERIM. First, a brief analysis of the C_n^2 profiles which was carried out to assess the validity of the analytical atmospheric model is presented. Then the results of an in-depth data analysis to predict SAR performance for most of the test flights is described. Finally, these results are summarized.

2.2.2.1 Analytical Model Examination

Refraction index constant profiles were calculated at the U.S. Department of Commerce from the index of refraction measurements. The calculations performed are derived from Eqs. 1 and 2 to be

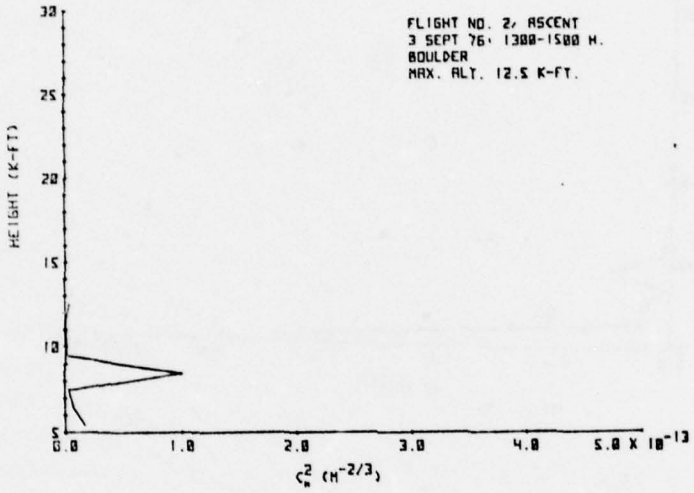


(a) Raw Index of Refraction Data Sample



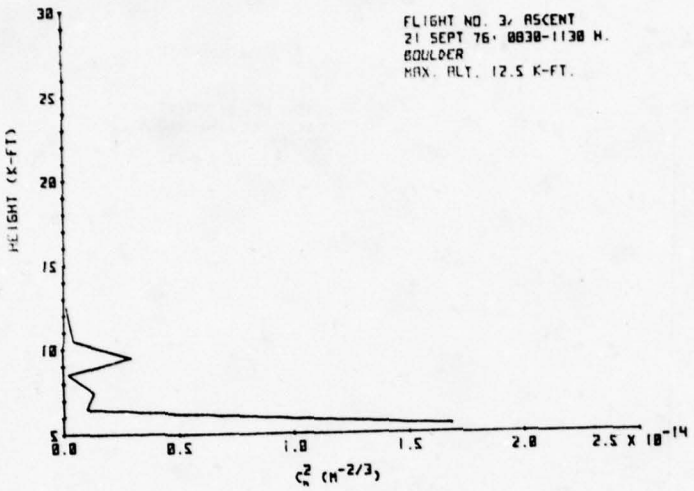
(b) Refractivity Profile Sample

Figure 11. Typical Index of Refraction Data from Flight 6A



FLIGHT 2, DESCENT (NO DATA)

Figure 12. Refractive Index Constant Profiles by Flight Number and Ascent (a) or Descent (d)



FLIGHT 3, DESCENT (NO DATA)

Figure 12. Refractive Index Constant Profiles by Flight Number and Ascent (a) or Descent (d) (continued)

FLIGHT 4, ASCENT (NO DATA)

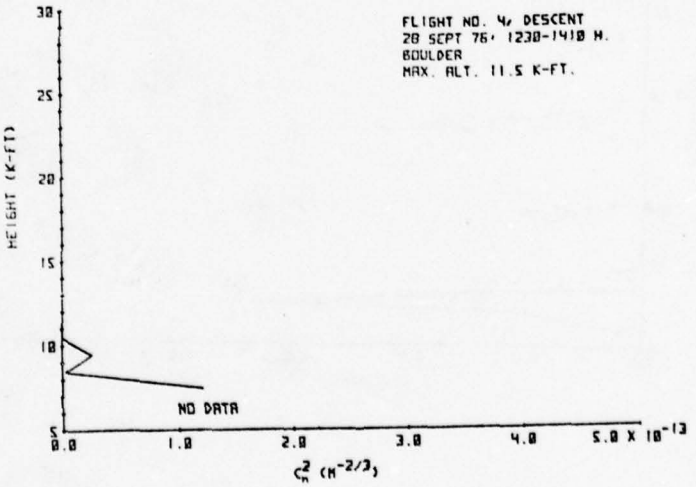
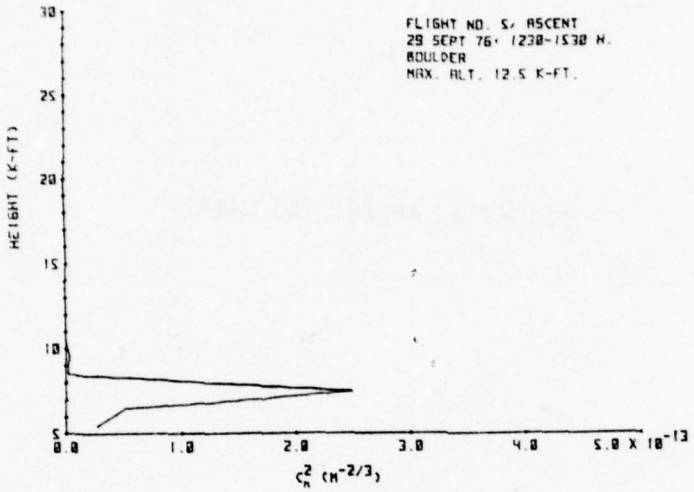


Figure 12. Refractive Index Constant Profiles by Flight Number and Ascent (a) or Descent (d) (continued)



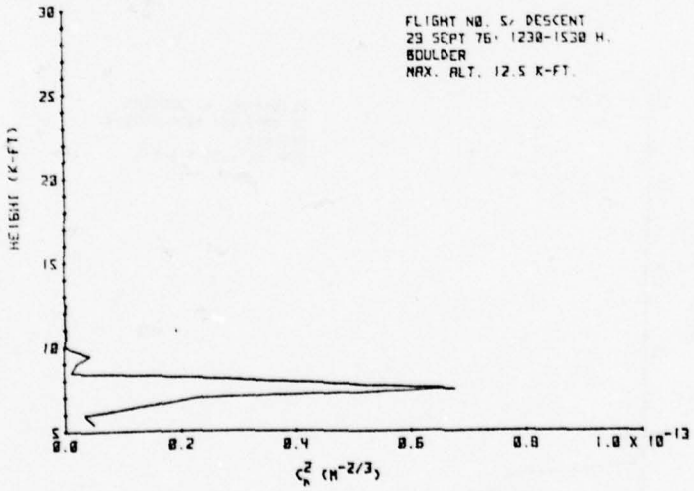
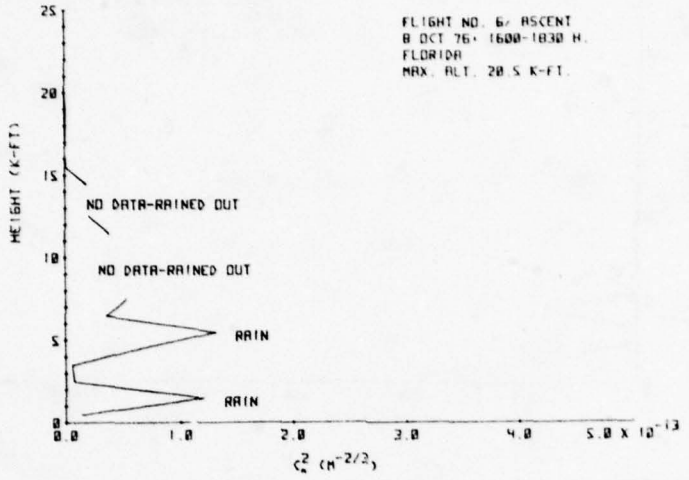


Figure 12. Refractive Index Constant Profiles by Flight Number and Ascent (a) or Descent (d) (continued)



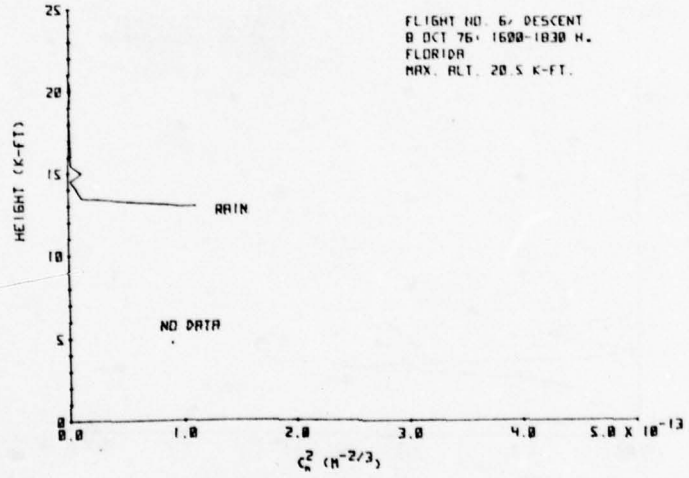
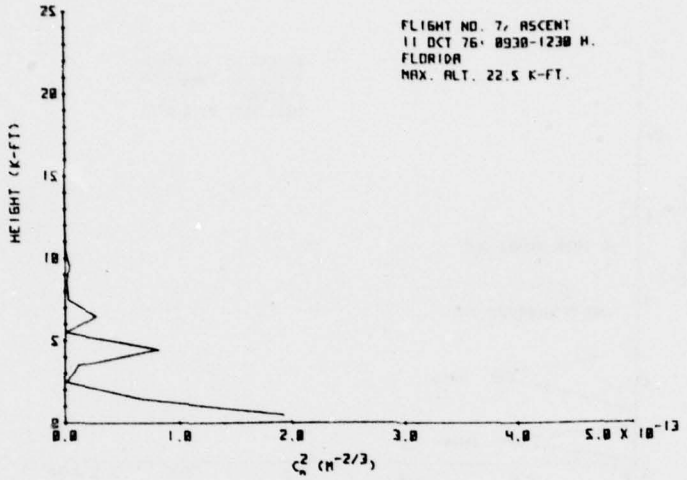


Figure 12. Refractive Index Constant Profiles by Flight Number and Ascent (a) or Descent (d) (continued)



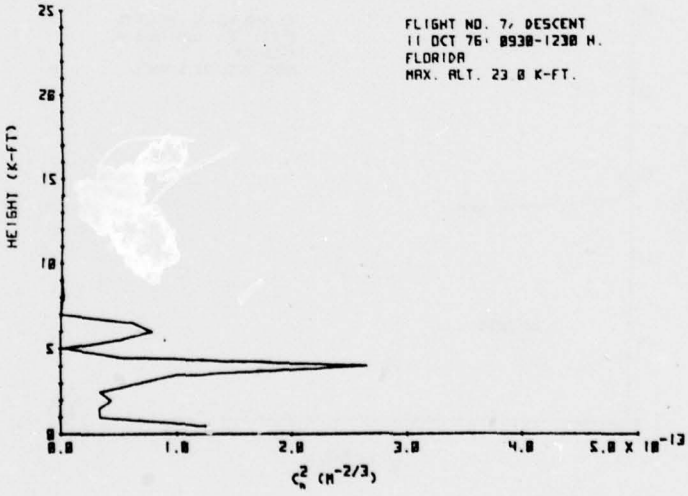
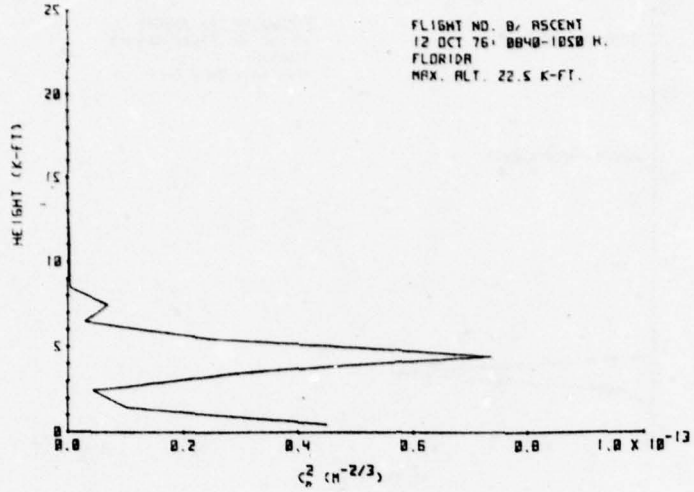


Figure 12. Refractive Index Constant Profiles by Flight Number and Ascent (a) or Descent (d) (continued)



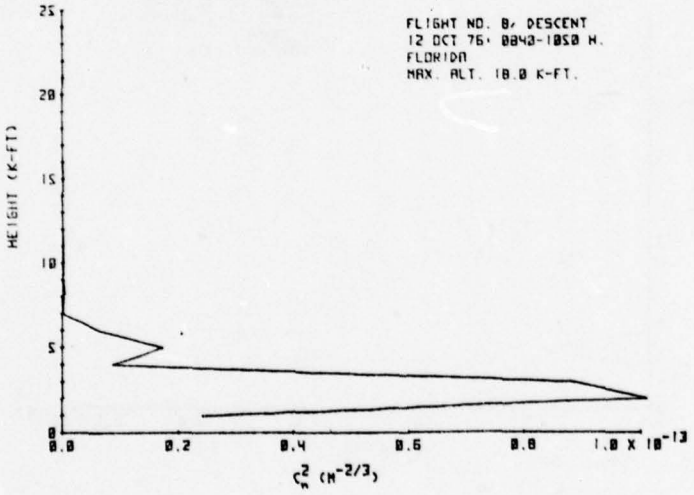
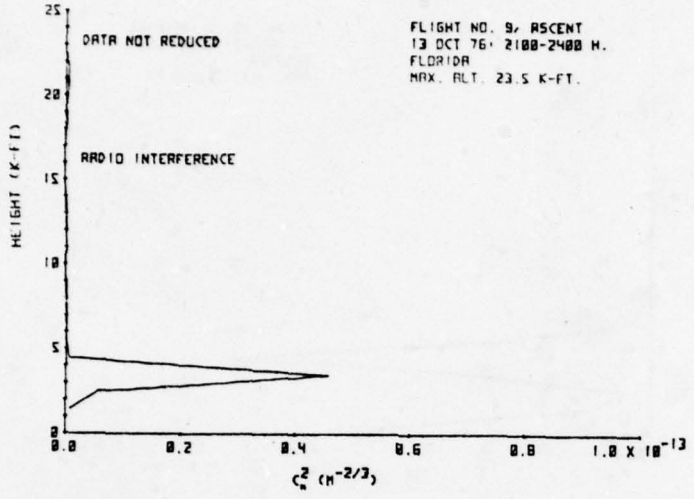


Figure 12. Refractive Index Constant Profiles by Flight Number and Ascent (a) or Descent (d) (continued)



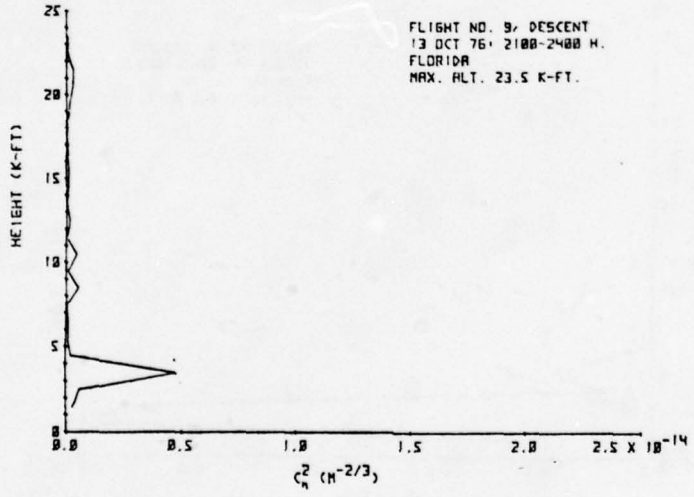
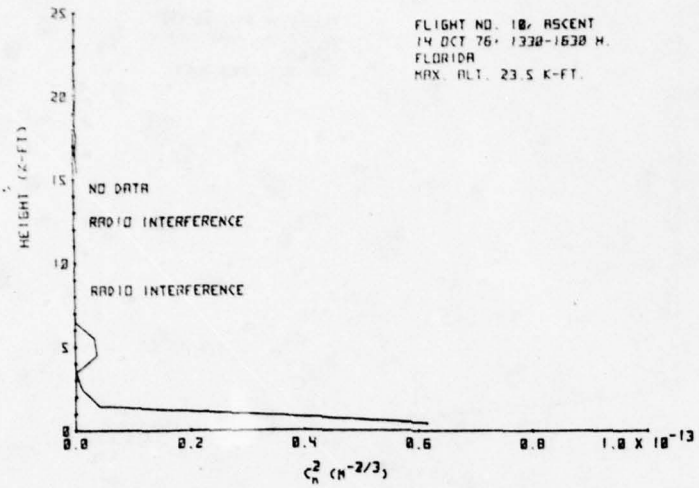


Figure 12. Refractive Index Constant Profiles by Flight Number and Ascent (a) or Descent (d) (continued)



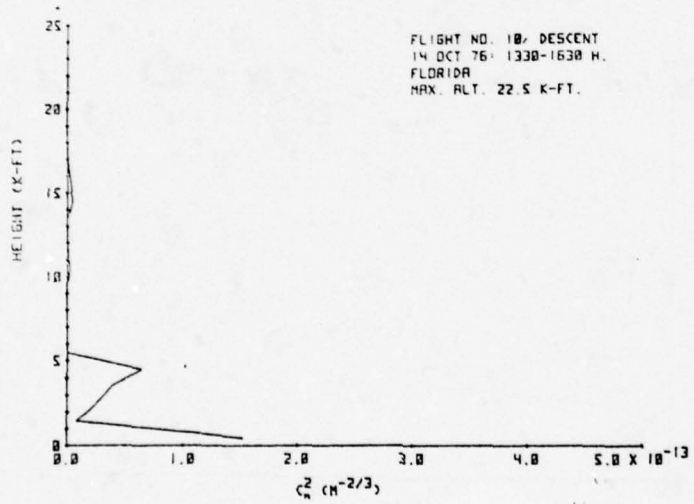
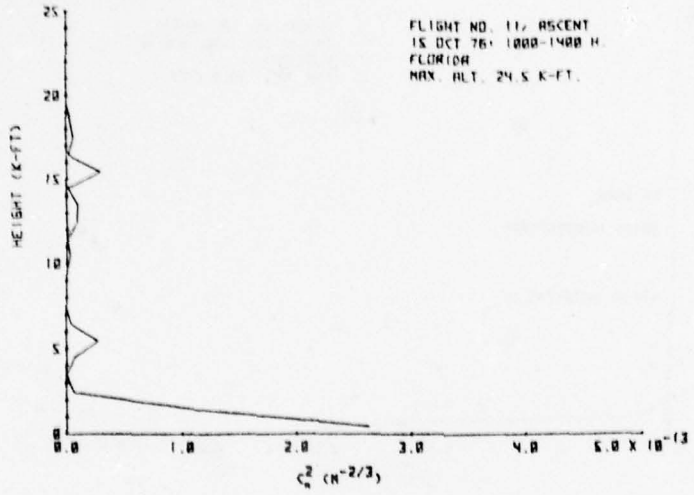


Figure 12. Refractive Index Constant Profiles by Flight Number and Ascent (a) or Descent (d) (continued)



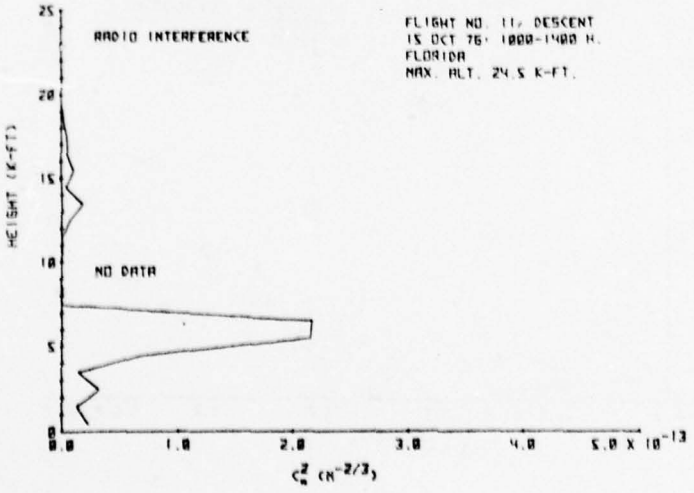
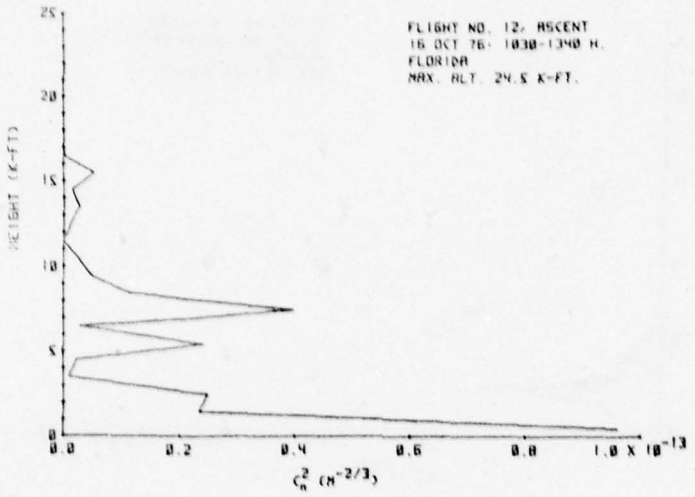


Figure 12. Refractive Index Constant Profiles by Flight Number and Ascent (a) or Descent (d) (continued)



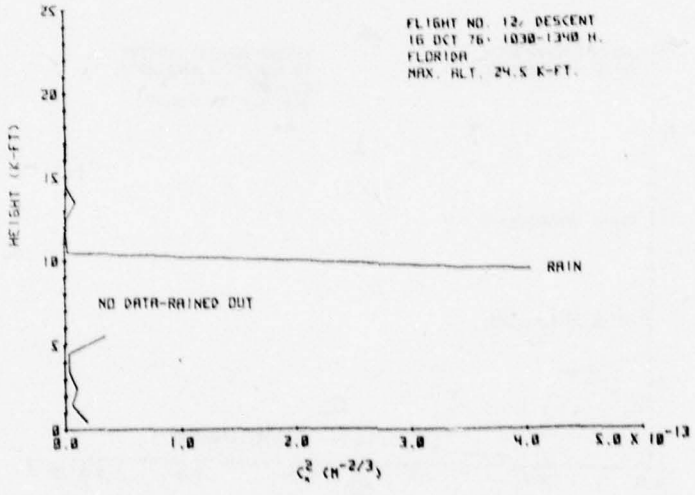
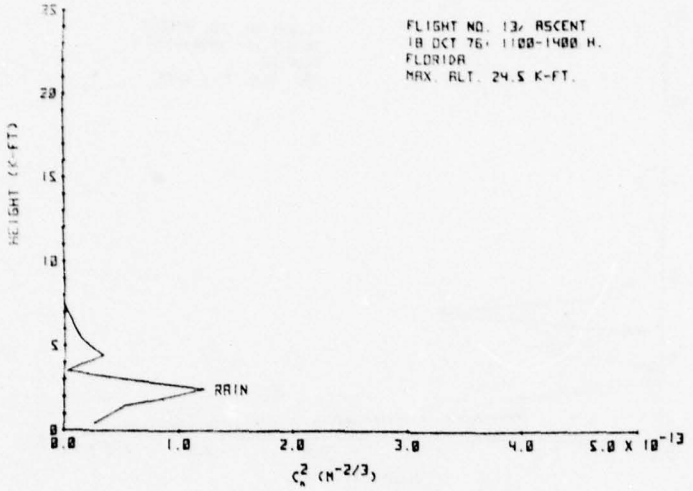


Figure 12. Refractive Index Constant Profiles by Flight Number and Ascent (a) or Descent (d) (continued)



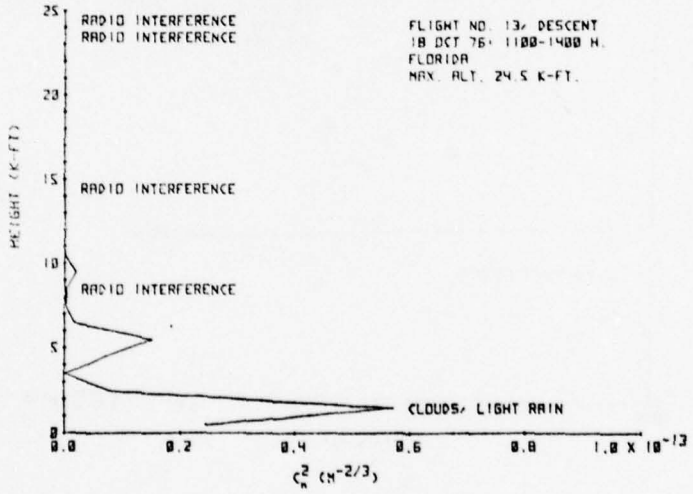
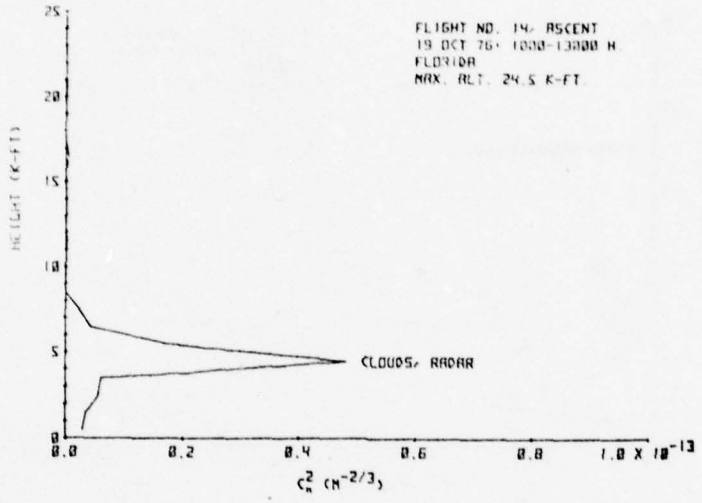


Figure 12. Refractive Index Constant Profiles by Flight Number and Ascent (a) or Descent (d) (continued)



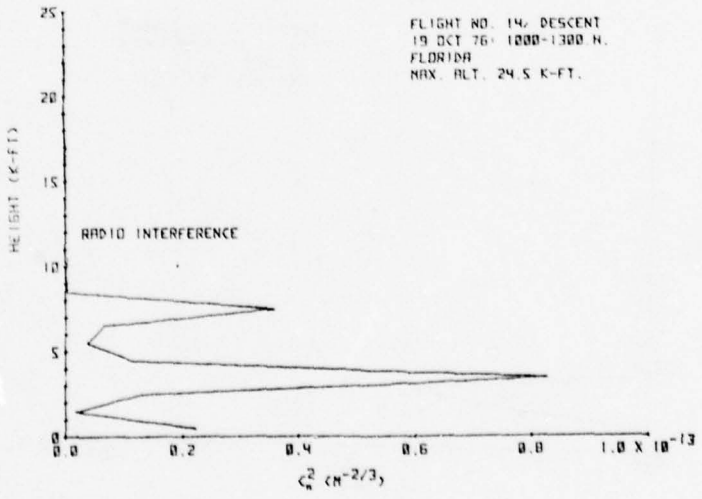
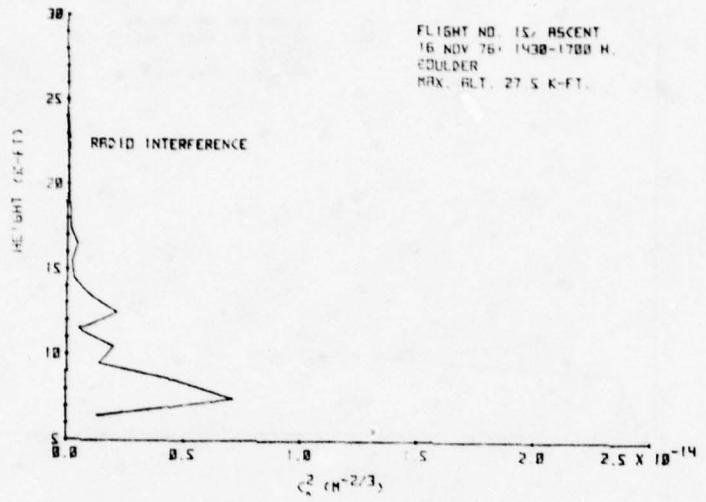


Figure 12. Refractive Index Constant Profiles by Flight Number and Ascent (a) or Descent (d) (continued)



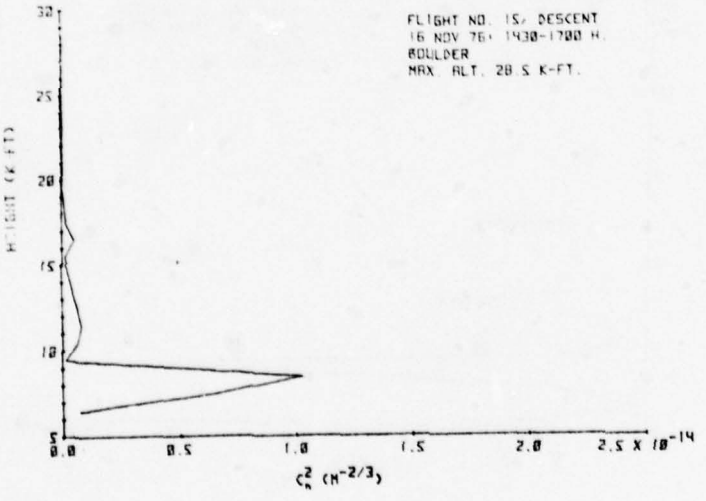
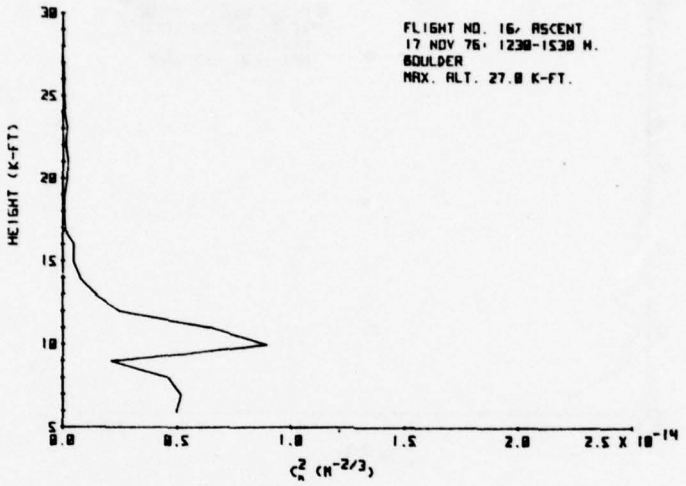


Figure 12. Refractive Index Constant Profiles by Flight Number and Ascent (a) or Descent (d) (continued)



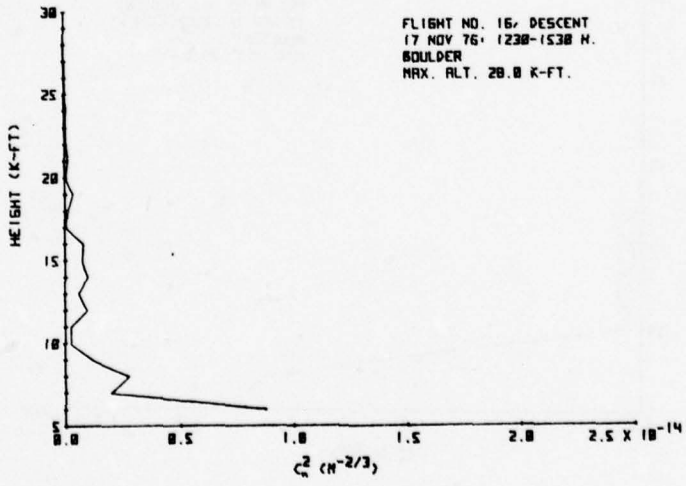
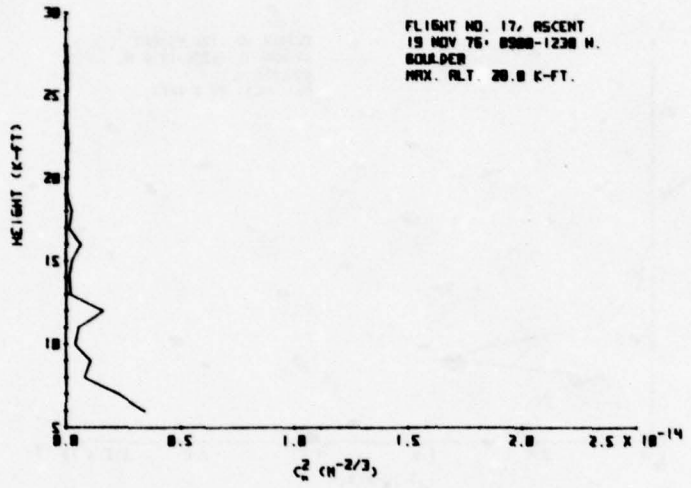


Figure 12. Refractive Index Constant Profiles by Flight Number and Ascent (a) or Descent (d) (continued)



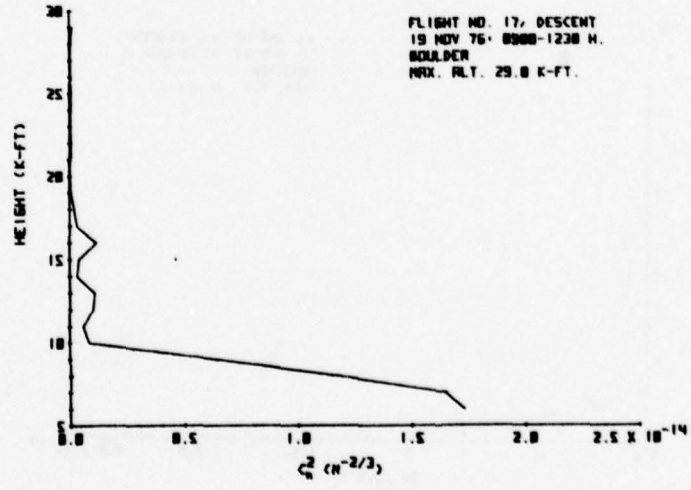


Figure 12. Refractive Index Constant Profiles by Flight Number and Ascent (a) or Descent (d) (concluded)

$$C_n^2(h) = \frac{1}{r^{2/3}} E[n(x + r) - n(x)]^2 \qquad (35)$$

These profiles were calculated for 1,000 ft, or on one occasion 500 ft, altitude intervals. As a test of the atmospheric turbulence model the value of C_n^2 was computed for values of path length r ranging between 10 and 500 meters. The calculated values must be independent of r and dependent only upon h in order for the model to be valid. Figure 13 shows two samples of these calculations. It is seen that the dependence upon the path length is indeed minimal and accordingly the model seems to be validated.

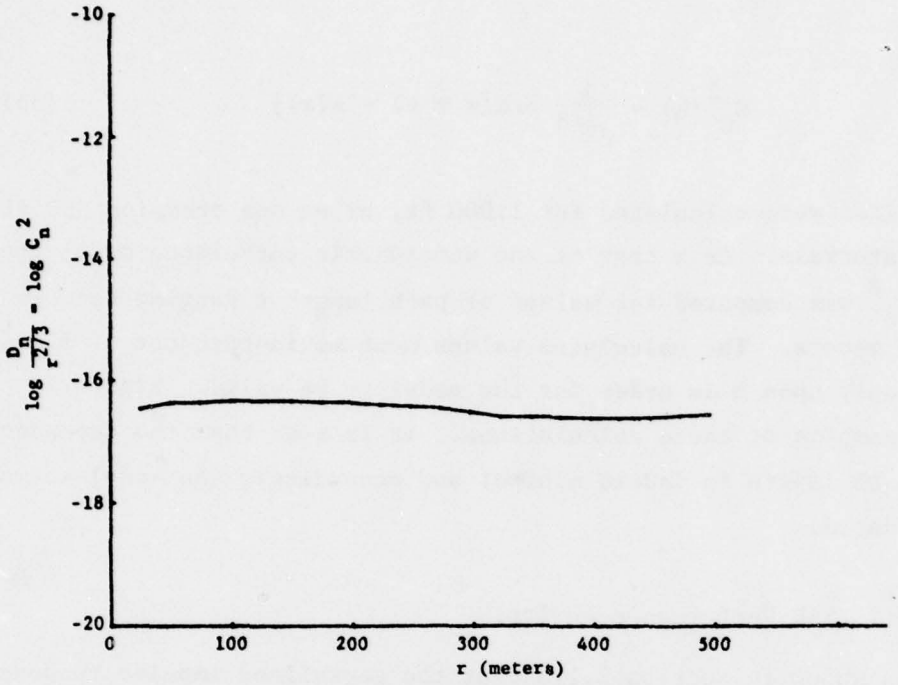
2.2.2.2 SAR Performance Analysis

It was shown in Section 2.1.3 that the normalized impulse response shape is characterized by the synthetic aperture phase error coefficient K_ϕ. From Eqs. 18 and 19 this coefficient may be written as

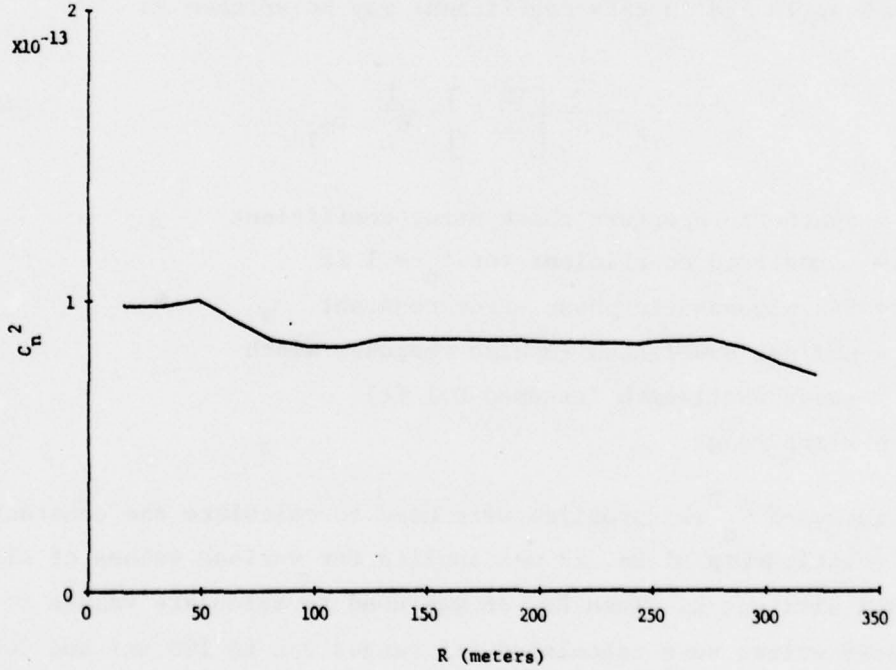
$$K_\phi = \frac{1}{\delta_o}\left[\frac{\lambda R}{4} C_\phi\right] = \frac{1}{\delta_o} K_{\phi_1} \qquad (36)$$

where K_ϕ = synthetic aperture phase error coefficient
K_{ϕ_1} = normalized coefficient for δ_o = 1 ft
C_ϕ = SAR atmospheric phase error constant
δ_o = nominal unweighted impulse response width
λ = radar wavelength (assumed 0.1 ft)
R = slant range

The measured $C_n^2(h)$ profiles were used to calculate the constant C_ϕ. The relationship of Eq. 13 was applied for various values of slant range R and altitude h. Then Eq. 36 was used to calculate values of K_{ϕ_1}. These values were calculated for ranges out to 100 nmi and for altitudes of 50, 70, and 90 thousand ft. Results of this data analysis



(a) Flight 6A, 20,500 ft.



(b) Variation in C_n^2 from Ref. 6

Figure 13. Dependence of C_n^2 on r

are presented in Figure 14. The value of wavelength used was 0.1 ft and the 4/3 earth radius model was used.

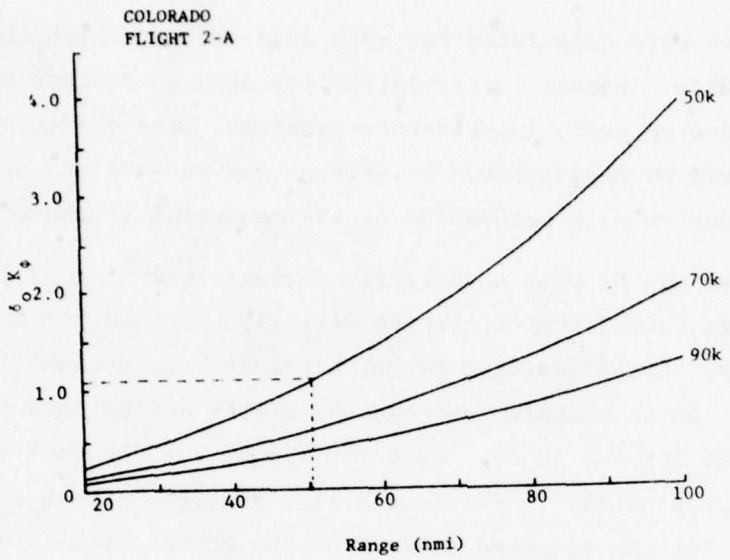
These curves were calculated for each data set for which complete data were available. Linear interpolation was used to replace data values missing due to radio interference problems. The effect of this replacement should be negligible. No attempt was made to use data with values missing due to rain saturation of the measuring instruments.

These curves can be used to directly estimate SAR imagery performance. The image coefficient K_ϕ can be directly obtained for any flight and any set of system parameters; range, altitude, and nominal impulse response width. As an example, suppose the system design is R = 50 miles, h = 50,000 ft, δ = 10 ft, then for flight 2-A the coefficient K_ϕ is simply approximately $\frac{1}{10} \times 1.1$ or 0.11. Thus the effect would be negligible even for the weighted case. For the worst case, flight 11D the same case yields $K_\phi \cong 0.42$. For the same flight, if the range was extended to 100 nmi the $K_\phi \cong 1.6$.

In an attempt to reduce the data even further three performance frequency plots were generated from the experimental data as shown in Figure 15. Each of the curves represents a quartile of the data computed from the 14 useable test flights. It should be emphasized that these plots are derived from limited data and cannot, in general, be used to predict specific SAR performance.

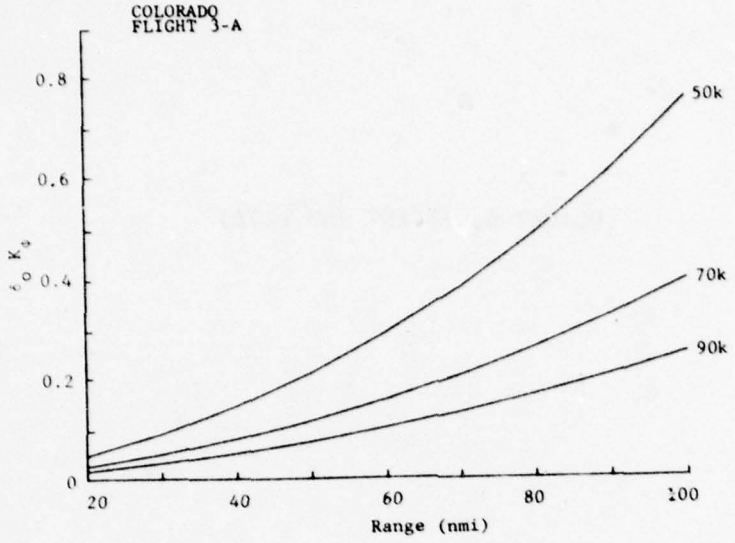
Curtis [8] uses a model that predicts SAR performance when surface water vapor pressure is known. The data analyzed herein was also examined to assess that model. Results were taken for an altitude of 50,000 ft and a range of 100 nmi. The scatter plot obtained is shown in Figure 16, each of the 14 Florida data flights is represented on this plot. The two quantities appear to be unrelated. The correlation coefficient was calculated to be 0.25.

From Eq. 12 it was shown that the factor effecting performance was $C_n^2(h)\, h^{5/3}$. Surface measurements probably should not be used alone. As $C_n^2(h)$ varies with altitude, the higher altitude values receive a



FLIGHT 2, DESCENT (NO DATA)

Figure 14. Normalized Synthetic Aperture Phase Error Coefficient, K_{ϕ_1}, for Experimental Data



FLIGHT 3, DESCENT (NO DATA)

Figure 14. Normalized Synthetic Aperture Phase Error Coefficient, K_{ϕ_1}, for Experimental Data (continued)

FLIGHT 4, ASCENT (NO DATA)

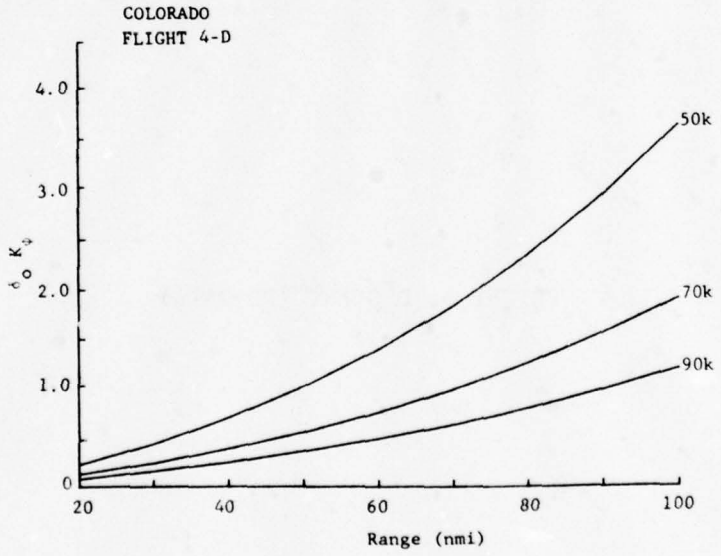
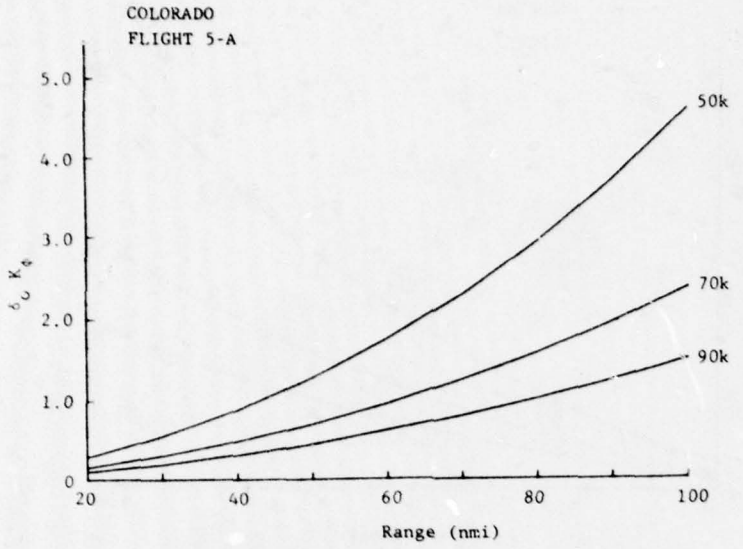


Figure 14. Normalized Synthetic Aperture Phase Error Coefficient, K_{ϕ_1}, for Experimental Data (continued)



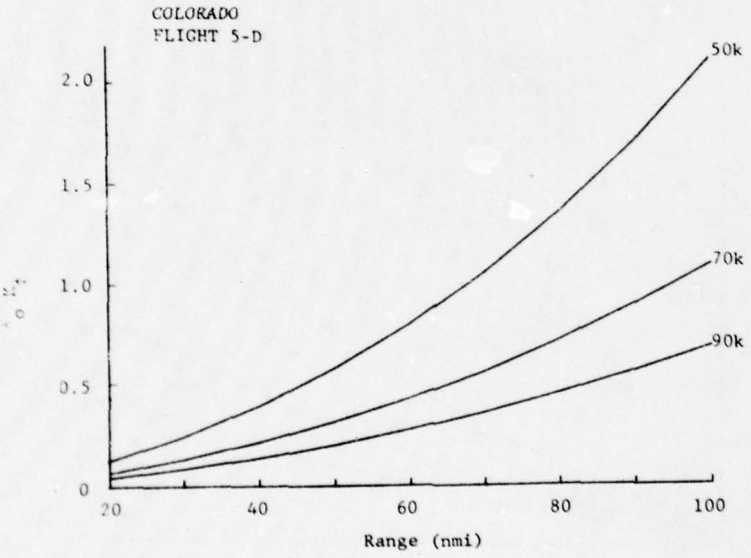
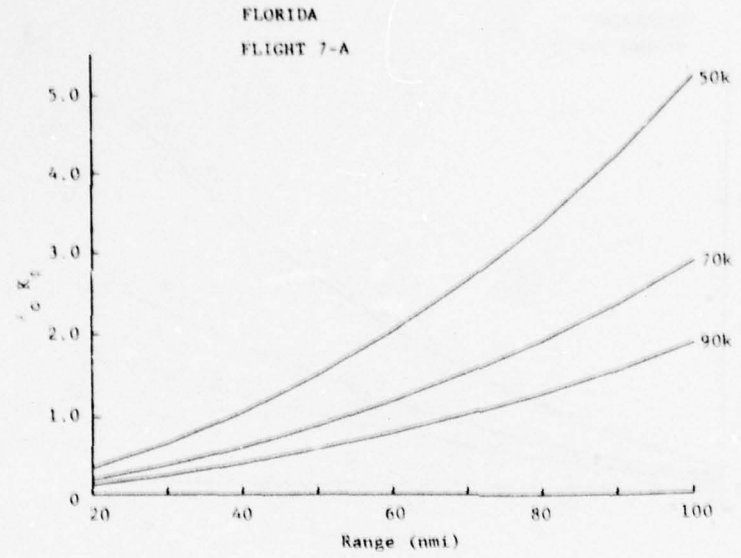


Figure 14. Normalized Synthetic Aperture Phase Error Coefficient, K_{ϕ_1}, for Experimental Data (continued)



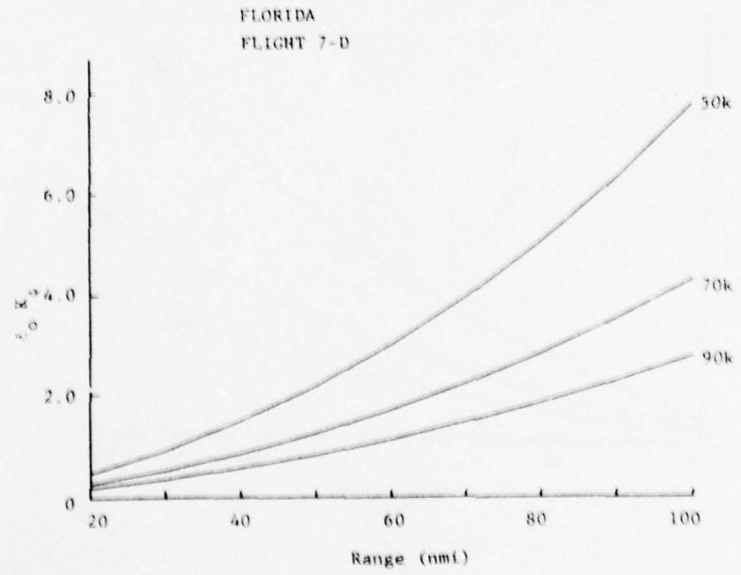
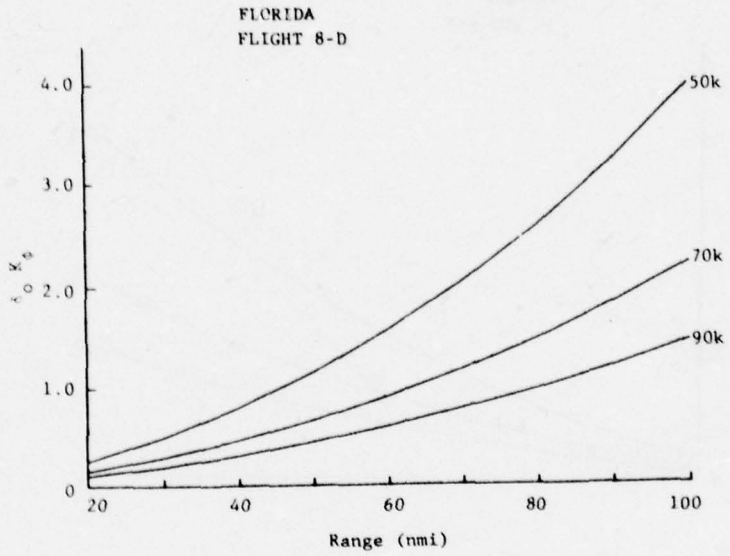
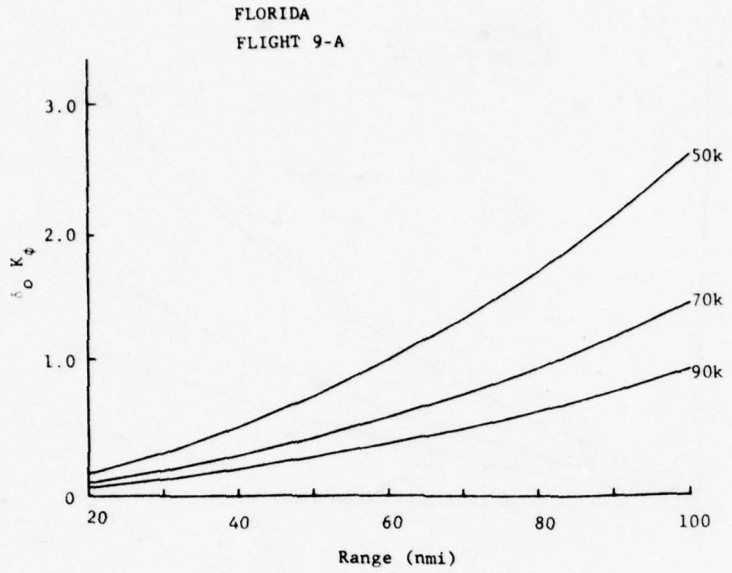


Figure 14. Normalized Synthetic Aperture Phase Error Coefficient, K_{ϕ_1}, for Experimental Data (continued)



FLIGHT 8, ASCENT (NO DATA)

Figure 14. Normalized Synthetic Aperture Phase Error Coefficient, K_{ϕ_1}, for Experimental Data (continued)



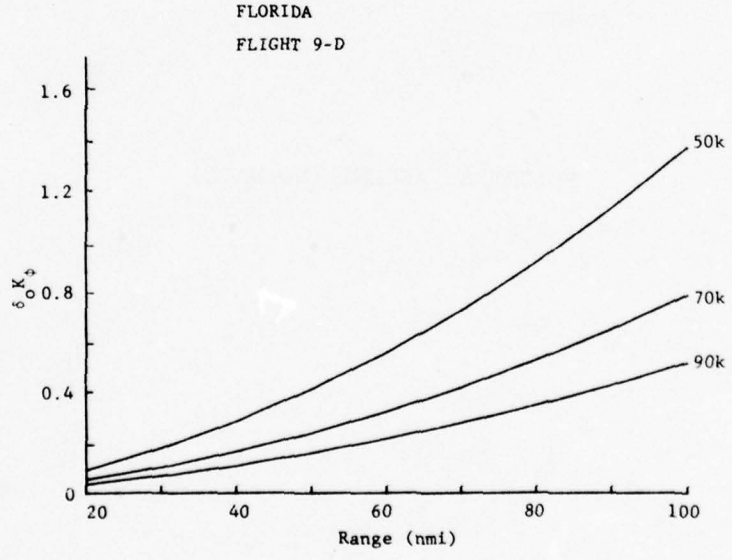
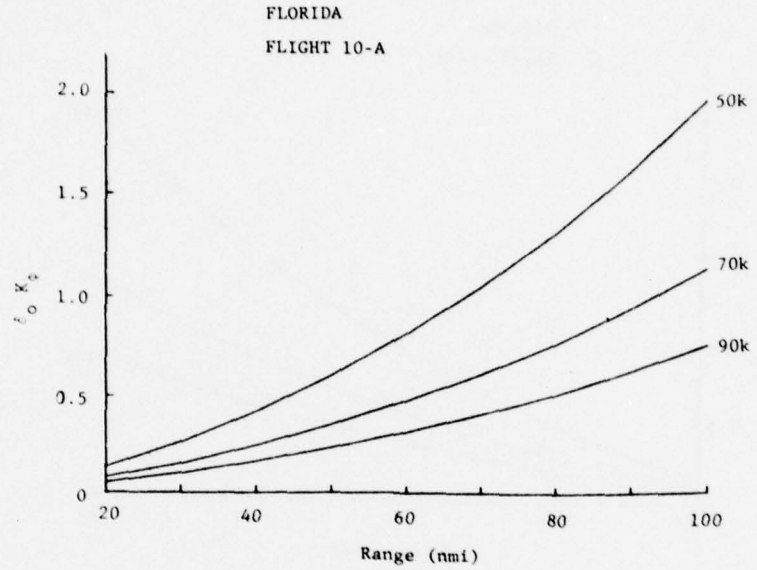


Figure 14. Normalized Synthetic Aperture Phase Error Coefficient, K_{ϕ_1}, for Experimental Data (continued)



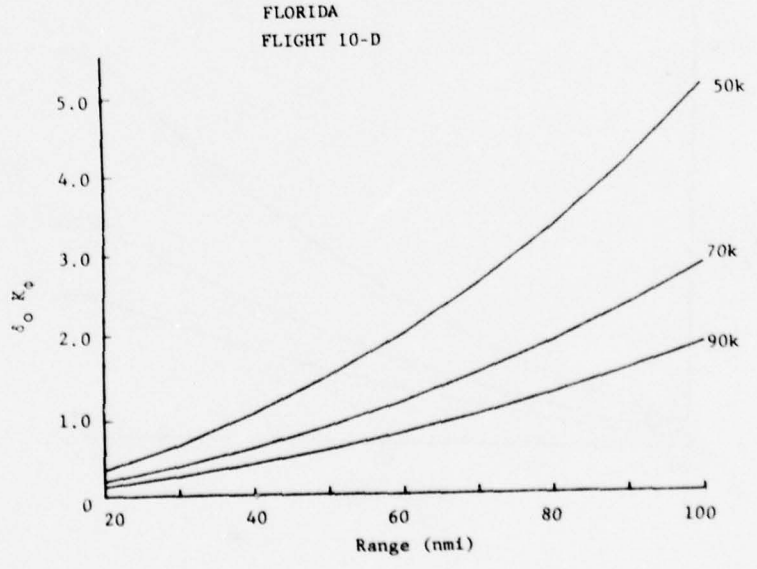
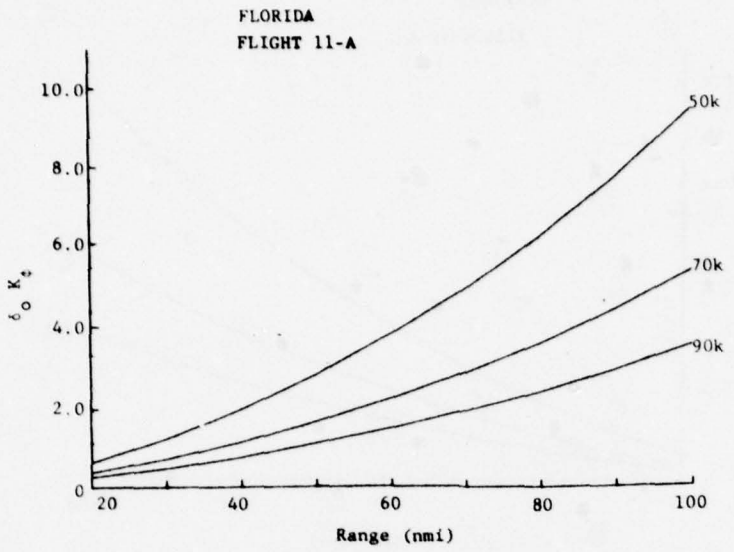


Figure 14. Normalized Synthetic Aperture Phase Error Coefficient, K_{ϕ_1}, for Experimental Data (continued)



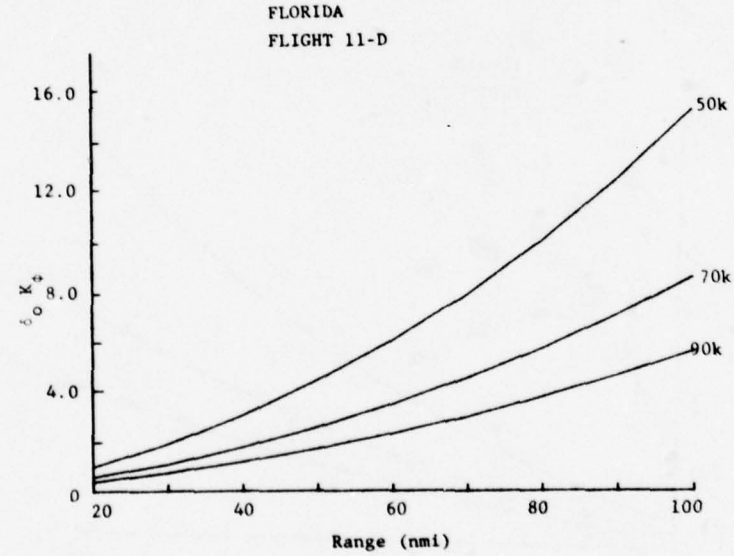
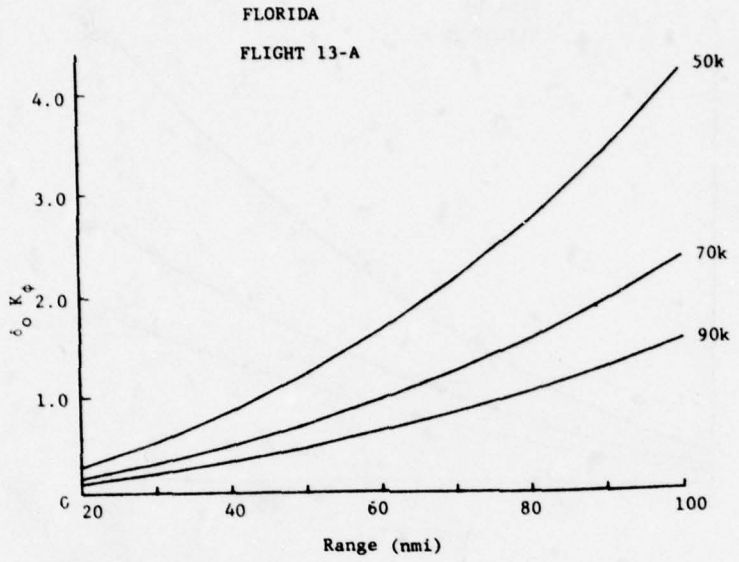


Figure 14. Normalized Synthetic Aperture Phase Error Coefficient, K_{ϕ_1}, for Experimental Data (continued)



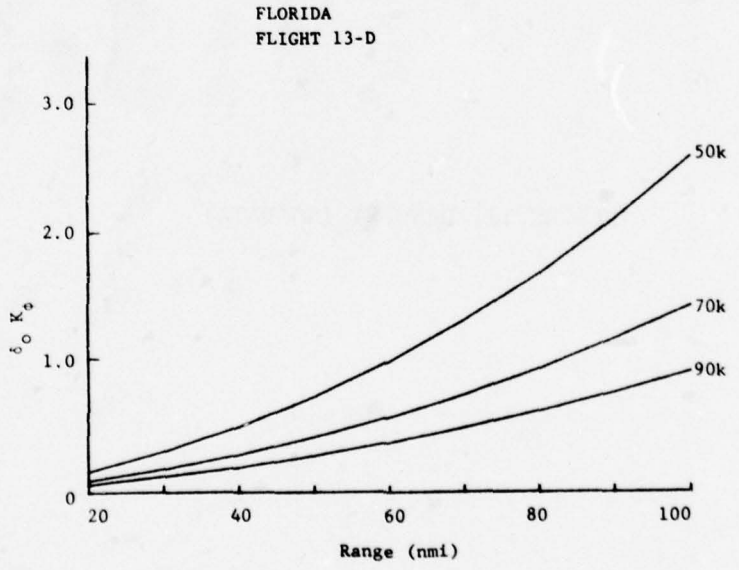
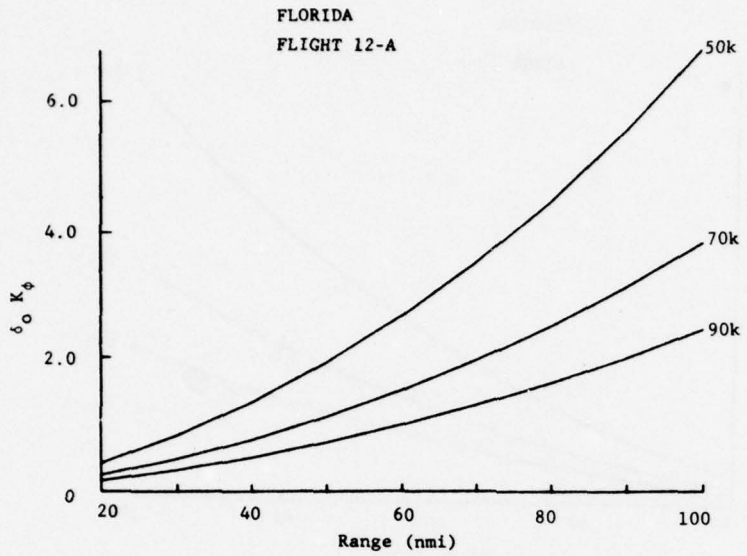
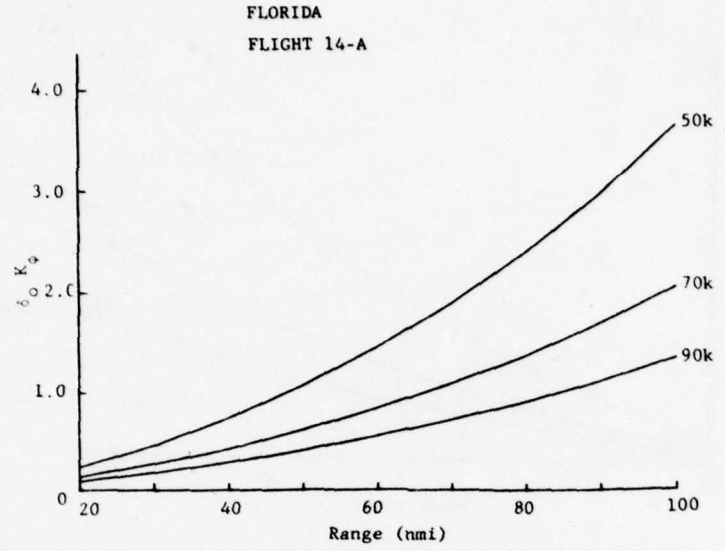


Figure 14. Normalized Synthetic Aperture Phase Error Coefficient, K_{ϕ_1}, for Experimental Data (continued)



FLIGHT 12, DESCENT (NO DATA)

Figure 14. Normalized Synthetic Aperture Phase Error Coefficient, K_{ϕ_1}, for Experimental Data (continued)



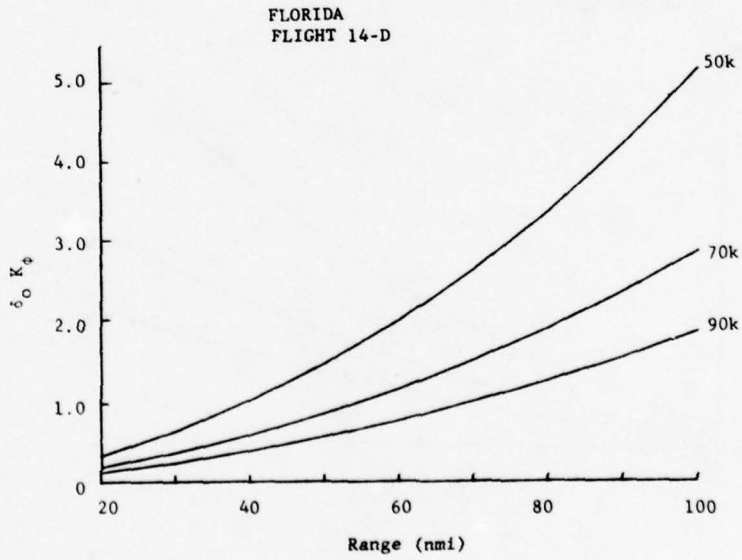
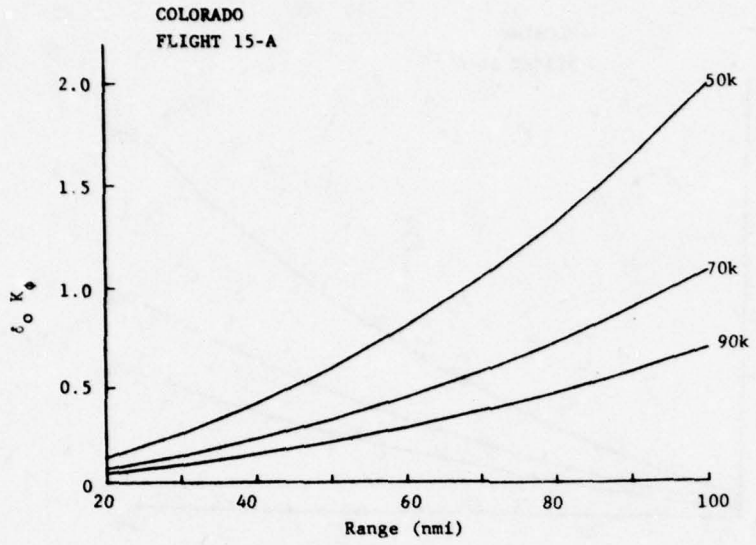


Figure 14. Normalized Synthetic Aperture Phase Error Coefficient, K_{ϕ_1}, for Experimental Data (continued)



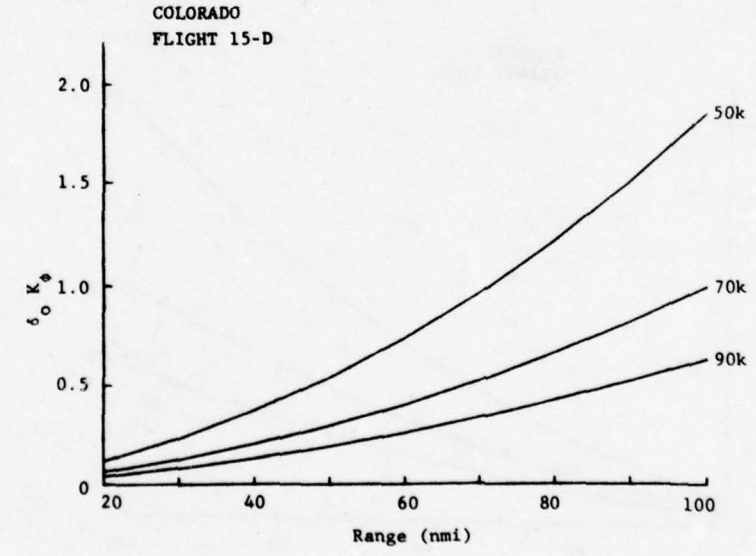
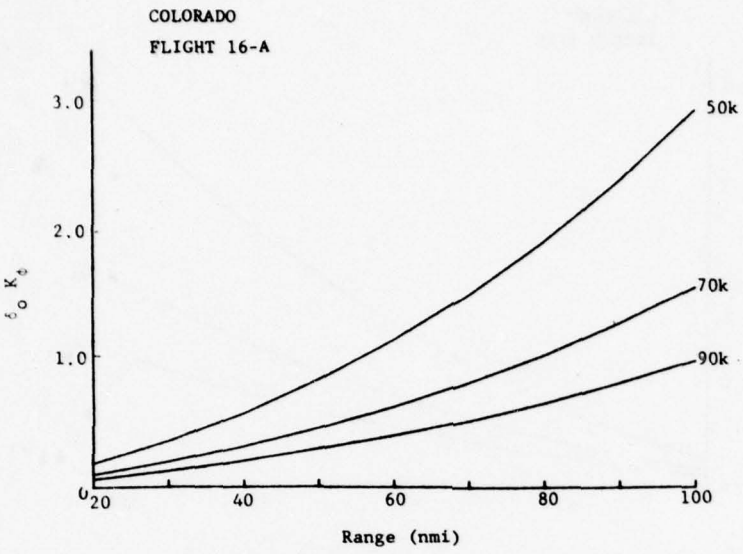


Figure 14. Normalized Synthetic Aperture Phase Error Coefficient, K_{ϕ_1}, for Experimental Data (continued)



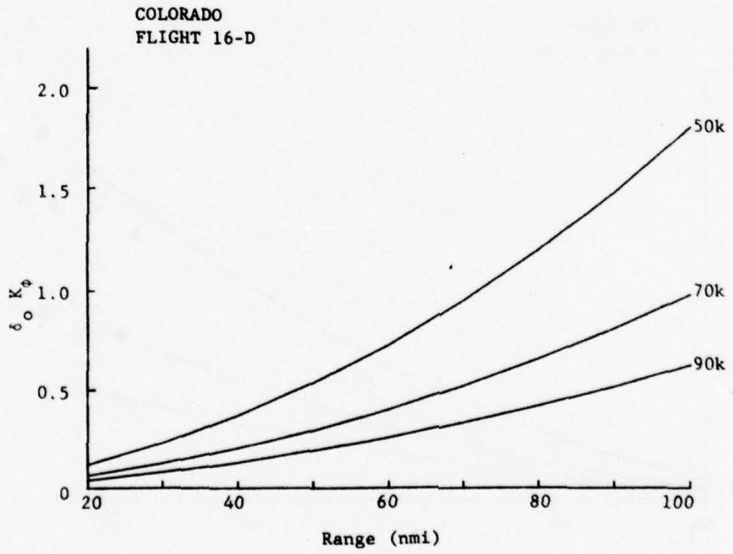
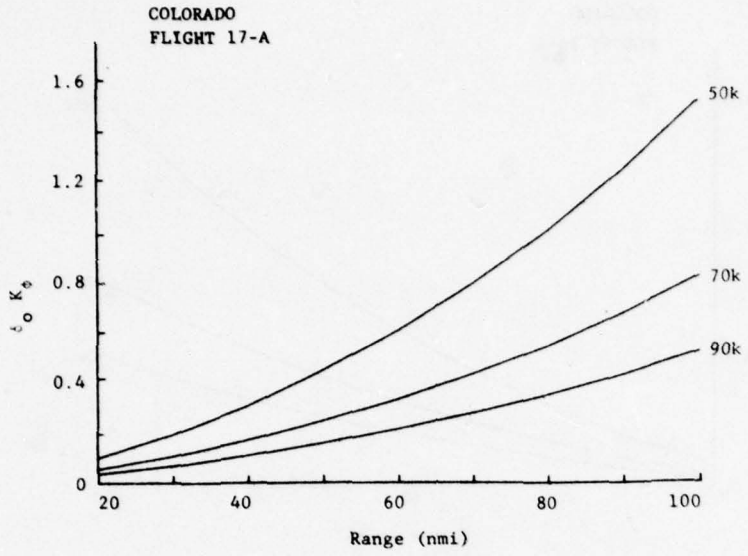


Figure 14. Normalized Synthetic Aperture Phase Error Coefficient, K_{ϕ_1}, for Experimental Data (continued)



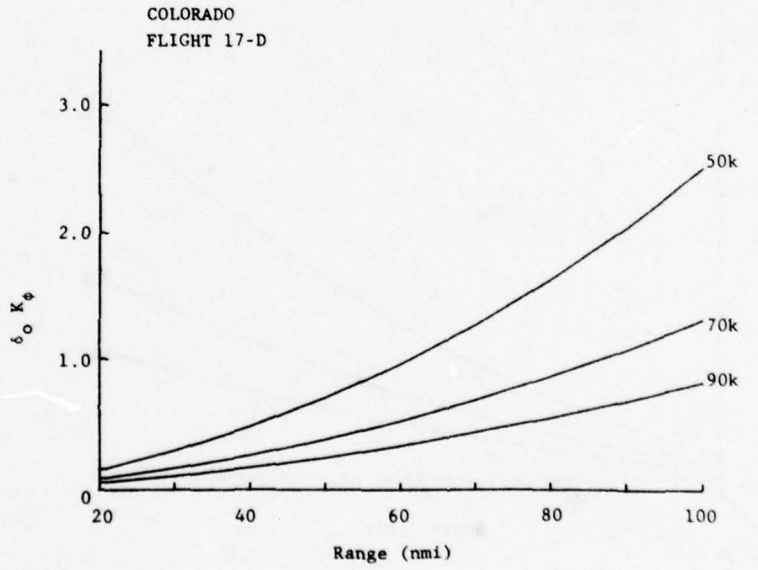


Figure 14. Normalized Synthetic Aperture Phase Error Coefficient, K_{ϕ_1}, for Experimental Data (concluded)

heavy weighting. The experimental data do exhibit significant disturbances at altitudes up to 10,000 ft.

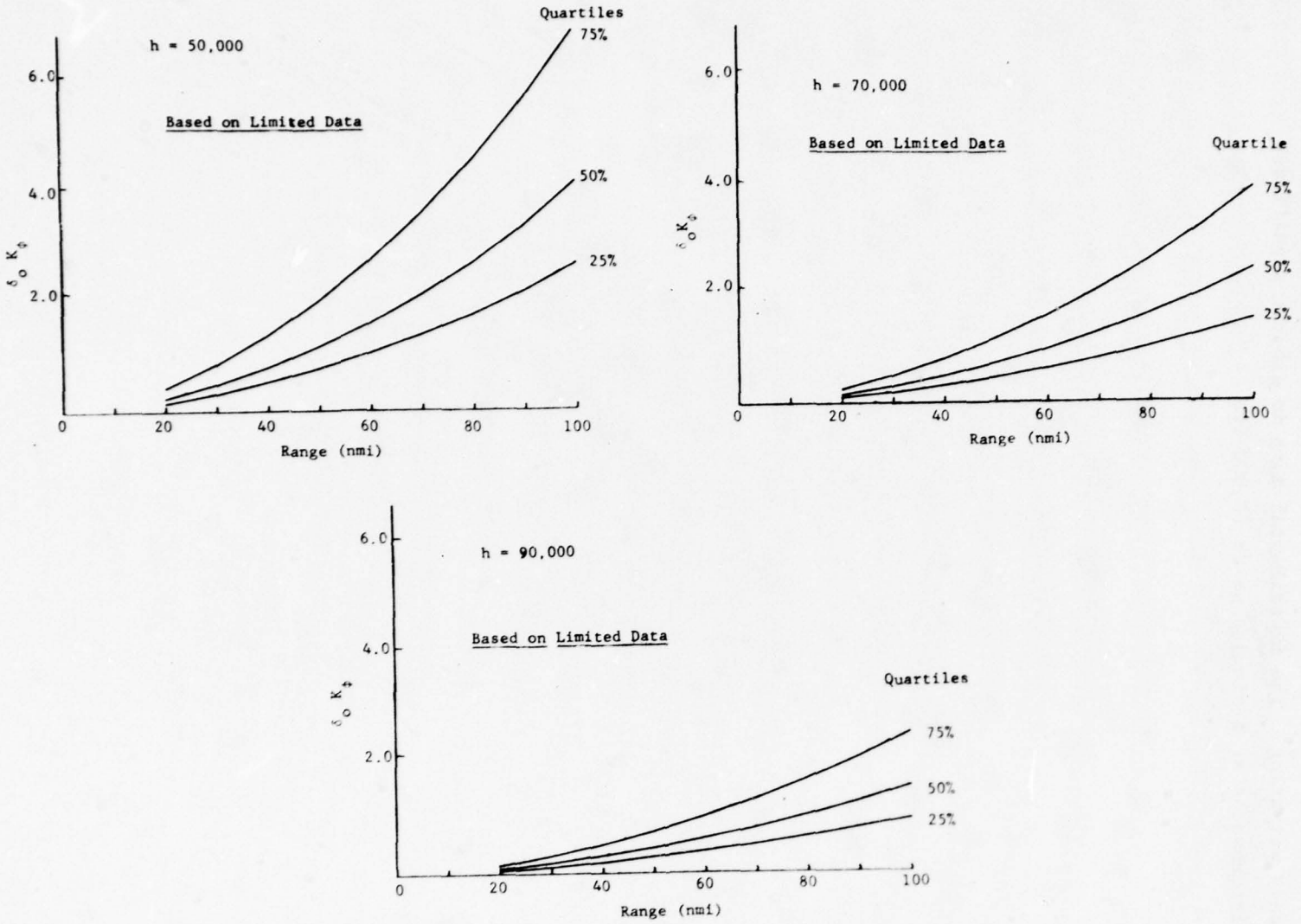


Figure 15. Frequency Plots for $\delta_o K_\phi$ Vs. Range, Altitude

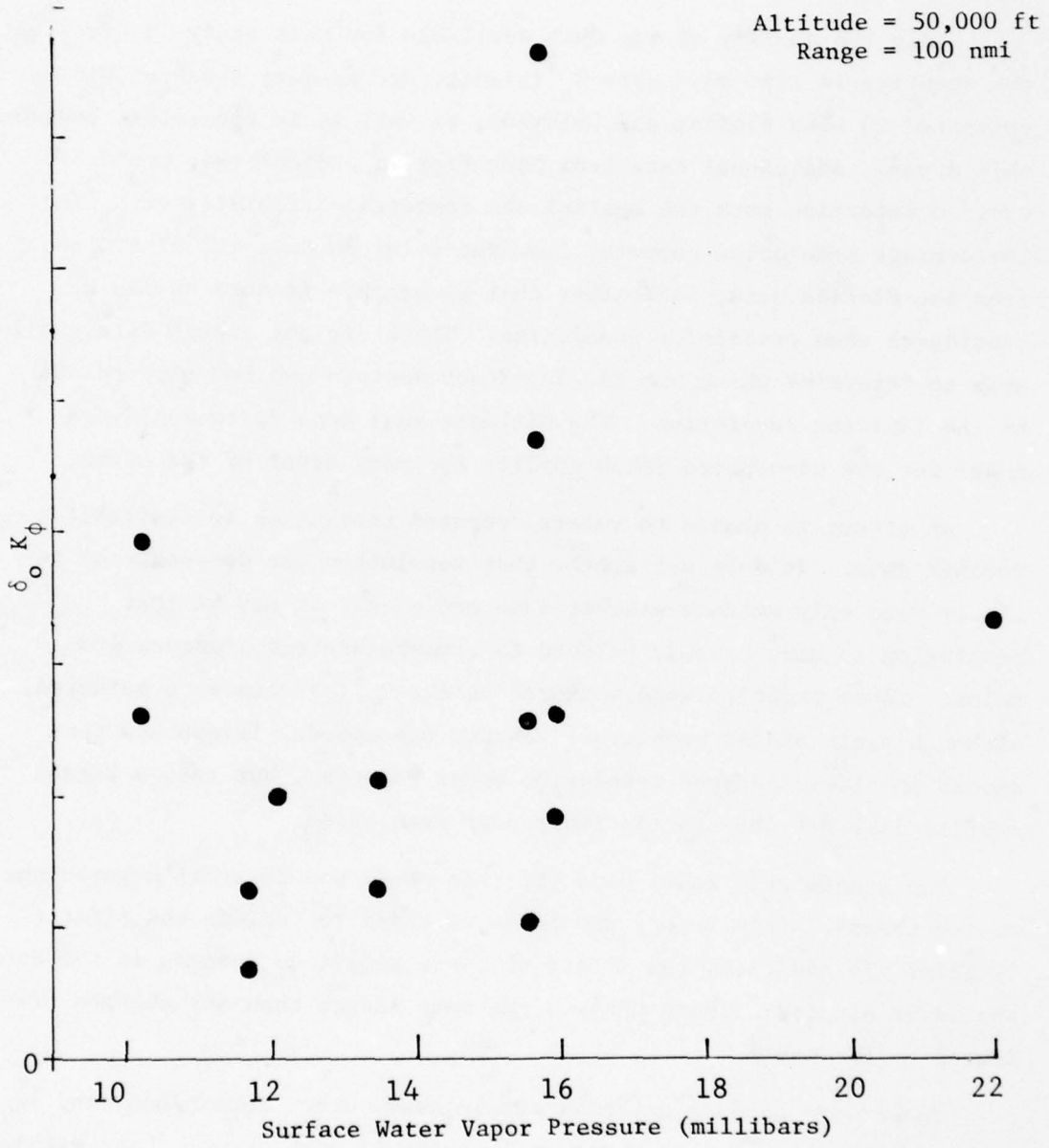


Figure 16. $\delta_o K_\phi$ Vs. Water Vapor Pressure

3
CONCLUSIONS AND RECOMMENDATIONS

While the quality of the data available for this study is excellent, the quantity is limited. More $C_n^2(h)$ data are needed; these should be collected in both Florida and Colorado, as well as in many other geographic areas. Additional data from both Florida and Colorado could be used to determine both the spatial and temporal variability of $C_n^2(h)$. The average resolution computed from the Colorado data was finer than from the Florida data, indicating that geographic factors should be considered when predicting resolution. There are not enough data available to determine which are the important factors and how they relate to the limiting resolution. The ultimate goal here is to achieve a model for the atmosphere which applies for many areas of the earth.

An effort is needed to relate computed resolution to available weather data. It does not appear that resolution can be predicted reliably when only surface weather data are used. It may be that resolution is more closely related to temperature and pressure profiles. These profiles were measured as the $C_n^2(h)$ data were gathered, although their use as predictors was not attempted. It appears that smooth profiles and good resolution occur together, but that a ragged profile does not necessarily imply poor resolution.

The atmospheric model used for this study was Tatarski's turbulent medium theory. This theory should be extended to include the effects of rain. In addition, the effect of large amplitude changes in the data should be studied. These changes are much larger than any changes predicted by the model.

There were no data gathered within heavy cloud formations, and it is not known whether this model would apply in such cases. Data within clouds should be collected and the usefulness of the model should be investigated.

APPENDIX A

AVERAGE POINT TARGET RESPONSE FIXED FOCUS

This appendix contains the derivation of the average point target azimuth response pattern for a synthetic aperture radar in the presence of atmospheric phase errors.

The radar response to a point target in the azimuth coordinate is modeled, from Eq. 16, as

$$f(x) = \int_{\frac{-L_s}{2}}^{\frac{L_s}{2}} A(u)\, e^{j\phi(u)}\, e^{-j\frac{4\pi xu}{\lambda R}}\, du \qquad \text{(A-1)}$$

The linear component of $\phi(u)$ does not affect the shape of the response, only its location. Therefore, the phase term will be expanded by

$$\gamma_1(u) = \phi(u) - m_1 u \qquad \text{(A-2)}$$

and the shape of the pattern will then be determined by evaluating

$$f(x) = \int_{\frac{-L_s}{2}}^{\frac{L_s}{2}} A(u)\, e^{j\gamma_1(u)}\, e^{-j\frac{4\pi xu}{\lambda R}}\, du \qquad \text{(A-3)}$$

First m_1 is chosen to minimize $\int_{\frac{-L_s}{2}}^{\frac{L_s}{2}} |\gamma_1(u)|^2\, du$.

To find m_1 we expand

$$\int_{\frac{-L_s}{2}}^{\frac{L_s}{2}} |\gamma_1(u)|^2 \, du = \int_{\frac{-L_s}{2}}^{\frac{L_s}{2}} [\phi(u) - m_1(u)]^2 \, du$$

$$= \frac{L_s^3}{12} m_1^2 - 2m_1 \int_{\frac{-L_s}{2}}^{\frac{L_s}{2}} u \, \phi(u) \, du + \int_{\frac{-L_s}{2}}^{\frac{L_s}{2}} \phi^2(u) \, du \quad \text{(A-4)}$$

Since the above sum is non-negative then the minimum occurs when

$$m_1 = \frac{12}{L_s^3} \int_{\frac{-L_s}{2}}^{\frac{L_s}{2}} u \, \phi(u) \, du \quad \text{(A-5)}$$

The factor

$$\frac{12}{L_s^3} \int_{\frac{-L_s}{2}}^{\frac{L_s}{2}} \phi(0) \, u \, du = 0$$

can be added to A-5 to yield

$$m_1 = \frac{12}{L_s^3} \int_{\frac{-L_s}{2}}^{\frac{L_s}{2}} u[\phi(u) - \phi(0)] \, du \quad \text{(A-6)}$$

The average point target response is then

$$E|f(x)|^2 = \int_{-\frac{L_s}{2}}^{\frac{L_s}{2}} \int_{-\frac{L_s}{2}}^{\frac{L_s}{2}} A(u)\,\bar{A}(v)\, e^{-j\frac{4\pi x(u-v)}{\lambda R}} E\left\{e^{j[\gamma_1(u)-\gamma_1(v)]}\right\} du\, dv \tag{A-7}$$

We now use the assumption that $\gamma_1(u) - \gamma_1(v)$ is Gaussian to write

$$E\left\{e^{j[\gamma_1(u)-\gamma_1(v)]}\right\} = e^{-\frac{1}{2}E[\gamma_1(u)-\gamma_1(v)]^2} = e^{-\frac{1}{2}D_{\gamma_1}(u-v)} \tag{A-8}$$

so that

$$E|f(x)|^2 = \frac{L_s^2}{4} \int_{-1}^{1}\int_{-1}^{1} A\left(\frac{L_s u}{2}\right)\bar{A}\left(\frac{L_s v}{2}\right) e^{-j\frac{2\pi L_s x(u-v)}{\lambda R}} e^{-\frac{1}{2}D_{\gamma_1}\left(\frac{L_s u}{2}-\frac{L_s v}{2}\right)} du\, dv \tag{A-9}$$

Next to find the structure function of $\gamma_1(x)$ in terms of the structure function of $\phi(x)$ we write

$$D_{\gamma_1}(x-y) = E\left\{[\gamma_1(x) - \gamma_1(y)]^2\right\}$$

$$= E\left\{[\phi(x) - \phi(y)]^2\right\} - 2(x-y)\, E\left\{m_1[\phi(x) - \phi(y)]\right\}$$

$$+ (x-y)^2\, E\left\{m_1^2\right\} \tag{A-10}$$

These three terms of A-10 will be evaluated separately.

First, $E\left\{[\phi(x) - \phi(y)]^2\right\} = D_\phi(x-y)$ (A-11)

Second, the identity

$$(a-b)\ (c-d) = \frac{1}{2}\left[(a-d)^2 + (b-c)^2 - (a-c)^2 - (b-d)^2\right] \qquad \text{(A-12)}$$

will be used to write

$$E\left\{m_1\left[\phi(x) - \phi(y)\right]\right\} = \frac{12}{L_s^3}\int_{-\frac{L_s}{2}}^{\frac{L_s}{2}} uE\left\{\left[\phi(u) - \phi(0)\right]\left[\phi(x) - \phi(y)\right]\right\}\, du$$

$$= \frac{6}{L_s^3}\int_{-\frac{L_s}{2}}^{\frac{L_s}{2}} uE\left\{\left[\phi(u) - \phi(y)\right]^2 + \left[\phi(0) - \phi(x)\right]^2 - \left[\phi(u) - \phi(x)\right]^2 - \left[\phi(\ ) - \phi(y)\right]^2\right\} du$$

$$= \frac{6}{L_s^3}\int_{-\frac{L_s}{2}}^{\frac{L_s}{2}} u\left[D_\phi(u-y) - D_\phi(u-x)\right] du$$

$$= \frac{3}{2L_s}\int_{-1}^{1} u\left[D_\phi\left(\frac{L_s}{2}\,u-y\right) - D_\phi\left(\frac{L_s}{2}\,u-x\right)\right] du \qquad \text{(A-13)}$$

Finally,

$$E\left[m_1^2\right] = \left(\frac{12}{L_s^3}\right)^2 \int_{-\frac{L_s}{2}}^{\frac{L_s}{2}}\int_{-\frac{L_s}{2}}^{\frac{L_s}{2}} xy\ E\left\{\left[\phi(x) - \phi(0)\right]\left[\phi(y) - \phi(0)\right]\right\} dx\, dy$$

continued on next page

$$= \frac{72}{L_s^6} \int_{-\frac{L_s}{2}}^{\frac{L_s}{2}} \int_{-\frac{L_s}{2}}^{\frac{L_s}{2}} xy\, E\Big\{\big[\phi(x) - \phi(0)\big]^2 + \big[\phi(0) - \phi(y)\big]^2$$

$$-\big[\phi(x) - \phi(0)\big]^2\Big\}^2 \, dx\, dy$$

$$= -\frac{9}{2L_s^2} \int_{-1}^{1} \int_{-1}^{1} xy\, D_\phi\left(\frac{L_s}{2}\, x - \frac{L_s}{2}\, y\right) dx\, dy \qquad \text{(A-14)}$$

When the three terms of A-10 are combined the result is

$$D_{\gamma_1}(x-y) = D_\phi(x-y) - (x-y)\,\frac{3}{L_s} \int_{-1}^{1} u\left[D_\phi\left(\frac{L_s}{2}\, u-y\right) - D_\phi\left(\frac{L_s}{2}\, u-x\right)\right] du$$

$$-\frac{9(x-y)^2}{2L_s^2} \int_{-1}^{1} \int_{-1}^{1} uv\, D_\phi\left(\frac{L_s}{2}\, u - \frac{L_s}{2}\, v\right) du\, dv \qquad \text{(A-15)}$$

This expression can be simplified by using the model for $D_\phi(r)$

$$D_\phi(r) = C_\phi^{5/3}\, |r|^{5/3} \qquad \text{(A-16)}$$

Then Eq. A-15 becomes

$$D_{\gamma_1}\left(\frac{L_s}{2}\,u - \frac{L_s}{2}\,v\right) = K_\phi^{5/3}\left\{|u-v|^{5/3}\right.$$

$$-\frac{3}{2}\,(u-v)\int_{-1}^{1} z\left[|z-v|^{5/3} - |z-u|^{5/3}\right]dz$$

$$\left.-\frac{9}{8}\,(u-v)^2\int_{-1}^{1}\int_{-1}^{1} xy|x-y|^{5/3}\,dx\,dy\right\} \qquad \text{(A-17)}$$

The two integrals above can be evaluated. The first is

$$\int_{-1}^{1} z|z-v|^{5/3}\,dz = \ell(v) - \ell(-v) \qquad \text{(A-18)}$$

where $\ell(v) = (1+v)^{8/3}\,\frac{9v-24}{88}$

The second is

$$\int_{-1}^{1}\int_{-1}^{1} xy|x-y|^{5/3}\,dx\,dy = -\frac{45}{187} \times 2^{5/3} \cong .764 \qquad \text{(A-19)}$$

Thus A-17 becomes

$$D_{\gamma_1}\left(\frac{L_s}{2}\,u - \frac{L_s}{2}\,v\right) = K_\phi^{5/3}\,q(u,v) \qquad \text{(A-20)}$$

where $q(u,v) = |u-v|^{5/3} + 0.86\,(u-v)^2$

$$+\frac{3}{2}\,(u-v)\left[\ell(v) - \ell(-v) - \ell(u) + \ell(-u)\right] \qquad \text{(A-21)}$$

The average point target response can thus be written, from Eqs. A-9 and A-20, as

$$E|f(x)|^2 = L_s^2 \, g\left(\frac{2L_s x}{\gamma R} \; ; \; K_\phi\right) \tag{A-22}$$

where $g(x;\, K_\phi) = \frac{1}{4}\int_{-1}^{1}\int_{-1}^{1} A\left(\frac{L_s}{2}\,u\right)\overline{A\left(\frac{L_s}{2}\,v\right)}\, e^{-j\pi(u-v)x}$

$$e^{-\frac{1}{2}K_\phi^{5/3} q(u,v)} \, du\, dv \tag{A-23}$$

If we set the weighting $A(u) = 1$ then

$$E|f(x)|^2 = L_s^2 \, g_1\left(\frac{2L_s x}{\lambda R} \; ; \; K_\phi\right) \tag{A-24}$$

where $g_1(x;\, K_\phi) = \frac{1}{4}\int_{-1}^{1}\int_{-1}^{1} e^{-j\pi(u-v)x} \, e^{-\frac{1}{2}K_\phi^{5/3} q(u,v)} \, du\, dv$ (A-25)

The function $g_1(x;\, K_\phi)$ has the following properties:

$$g_1(x;\, 0) = \left(\frac{\sin \pi x}{\pi x}\right)^2 \tag{A-26}$$

and

$$\int_{-\infty}^{\infty} g_1(x;\, K_\phi)\, dx = 1 \tag{A-27}$$

The function g_1 has been evaluated for a range of values of x between 0 and 6 and for values of K between 0 and 6.7. The results are shown in Figures 5 and 6.

If we set the amplitude weighting to be a cosine squared weighting then

$$E|f(x)|^2 = L_s^2 \, g_3\left(\frac{2L_s x}{\lambda R} \; ; \; K_\phi\right) \tag{A-28}$$

where $g_3(x; K_\phi) = \frac{1}{4} \int_{-1}^{1}\int_{-1}^{1} \cos^2\left[\frac{\pi}{2}(u-v)\right]$ (A-29)

$$e^{-j\pi(u-v)x} \; e^{-\frac{1}{2}K_\phi^{5/3} q(u-v)} \, du \, dv$$

This has been evaluated and is shown in Figure 7.

APPENDIX B

AVERAGE POINT TARGET RESPONSE CORRECTED FOCUS

This appendix contains the derivation of the average point target azimuth response pattern for a synthetic aperture radar in the presence of atmospheric phase errors with optimum focussing.

The analysis in this appendix is very similar to that in the previous appendix. The phase term to be expanded is

$$\gamma_2(u) = \phi(u) - m_1 u - m_2 u^2 \tag{B-1}$$

To find m_1 and m_2 to minimize

$$\int_{-\frac{L_s}{2}}^{\frac{L_s}{2}} |\gamma_2(u)|^2 \, du$$

we expand

$$\int_{-\frac{L_s}{2}}^{\frac{L_s}{2}} |\gamma_2(u)|^2 \, du = \frac{L_s^3}{12} m_1^2 - 2m_1 \int_{-\frac{L_s}{2}}^{\frac{L_s}{2}} u\phi(u) \, du +$$

$$+ \int_{-\frac{L_s}{2}}^{\frac{L_s}{2}} du - 2m_2 \int_{-\frac{L_s}{2}}^{\frac{L_s}{2}} u^2 (u) - m_2^2 \frac{L_s^5}{80} \tag{B-2}$$

The minimum value is when

$$m_1 = \frac{12}{L_s^3} \int_{-\frac{L_s}{2}}^{\frac{L_s}{2}} u\phi(u)\, du \qquad \text{(B-3)}$$

and

$$m_2 = \frac{80}{L_s^5} \int_{-\frac{L_s}{2}}^{\frac{L_s}{2}} u^2\phi(u)\, du \qquad \text{(B-4)}$$

As before we will evaluate $D_{\gamma_2}(x-y)$.

$$D_{\gamma_2}(x-y) = E\left\{\left[\gamma_2(x) - \gamma_2(y)\right]^2\right\}$$

$$= E\left\{\left[\phi(x) - \phi(y) - m_1(x-y) - m_2(x^2-y^2)\right]^2\right\}$$

$$= E\left\{\left[\phi(x) - \phi(y) - m_1(x-y)\right]^2\right.$$

$$-2(x^2-y^2)\, m_2\left[\phi(x) - \phi(y) - m_1(x-y)\right]$$

$$\left. + m_2^2(x^2-y^2)^2\right\} \qquad \text{(B-5)}$$

These three terms must be evaluated. The first was previously evaluated in Appendix A. The first portion of the second term is

$$E\left\{m_2\left[\phi(x) - \phi(y)\right]\right\} = E\left\{\frac{80}{L_s^5}\int_{-\frac{L_s}{2}}^{\frac{L_s}{2}} z^2\,\phi(z)\left[\phi(x) - \phi(y)\right]\,dz\right\}$$

$$= E\left\{\frac{80}{L_s^5}\int_{-\frac{L_s}{2}}^{\frac{L_s}{2}} z^2\left[\phi(z) - \phi(0)\right]\left[\phi(x) - \phi(y)\right]\,dz\right\} \qquad \text{(B-6)}$$

since

$$E[\phi(x) - \phi(y)] = 0 \qquad \text{(B-7)}$$

Using the identity in Appendix A, this becomes

$$E\left\{m_2\left[\phi(x) - \phi(y)\right]\right\} = E\left\{\frac{40}{L_s^5}\int_{-\frac{L_s}{2}}^{\frac{L_s}{2}} z^2\left[\phi(z) - \phi(y)\right]^2 + \left[\phi(0) - \phi(x)\right]^2 - \left[\phi(z) - \phi(x)\right]^2 - \left[\phi(0) - \phi(y)\right]^2\right\} dz$$

$$= \frac{40}{L_s^5}\int_{-\frac{L_s}{2}}^{\frac{L_s}{2}} z^2\left[D_\phi(z-y) + D_\phi(x) - D_\phi(z-x) - D_\phi(y)\right]\,dz \qquad \text{(B-8)}$$

$$= \frac{10}{3L_s^2}\left[D_\phi(x) - D_\phi(y)\right] + \frac{5}{L_s^2}\int_{-1}^{1} z^2\left[D_\phi\left(\frac{L_s}{2}\,z - y\right) - D_\phi\left(\frac{L_s}{2}\,z - x\right)\right]dz \qquad \text{(B-9)}$$

The remainder of the second term is

$$E\left\{2(x^2-y^2)\ m_2 m_1(x-y)\right\} = 0 \qquad \text{(B-10)}$$

since $E[m_1 m_2] = 0$

For the third term

$$E\left[m_2{}^2\right] = E\left\{\left(\frac{80}{L_s{}^5}\right)^2 \int_{-\frac{L_s}{2}}^{\frac{L_s}{2}} \int_{-\frac{L_s}{2}}^{\frac{L_s}{2}} x^2\ y^2\ \phi(x)\ \phi(y)\ dx\ dy\right\}$$

$$= \left(\frac{80}{L_s{}^5}\right)^2 \int_{-\frac{L_s}{2}}^{\frac{L_s}{2}} \int_{-\frac{L_s}{2}}^{\frac{L_s}{2}} x^2\ y^2\ E\left\{\left[\phi(x) - \phi(0)\right]\left[\phi(y) - \phi(0)\right]\right\} dx\ dy \qquad \text{(B-11)}$$

Since $E[\phi(x) - \phi(0)] = E[\phi(y) - \phi(0)] = 0$

The algebraic identity yields

$$E\left[m_2{}^2\right] = \frac{1}{2}\left(\frac{80}{L_s{}^5}\right)^2 \int_{-\frac{L_s}{2}}^{\frac{L_s}{2}} \int_{-\frac{L_s}{2}}^{\frac{L_s}{2}} x^2\ y^2\ E\left\{\left[\phi(x) - \phi(0)\right]^2\right.$$

$$\left. + \left[\phi(0) - \phi(y)\right]^2 - \left[\phi(x) - \phi(y)\right]^2\right\} dx\ dy$$

(continued on next page)

$$= \frac{50}{L_s^4} \int_{-1}^{1}\int_{-1}^{1} x^2 y^2 \left[D_\alpha\left(\frac{L_s}{2} x\right) + D_\alpha\left(\frac{L_s}{2} y\right) \right.$$

$$\left. - D_\alpha\left(\frac{L_s}{2} x - \frac{L_s}{2}\right) \right] dx\, dy \qquad \text{(B-12)}$$

After combining all terms we have

$$D_{\gamma_2}(x-y) = D_{\gamma_1}(x-y) - 2(x^2-y^2) \left\{ \frac{10}{3L_s^2} \left[D_\phi(x) - D_\phi(y) \right] \right.$$

$$\left. + \frac{5}{L_s^2} \int_{-1}^{1} z^2 \left[D_\phi\left(\frac{L_s}{2} z-y\right) - D_\phi\left(\frac{L_s}{2} z-x\right) \right] dz \right\}$$

$$+ (x^2-y^2)^2 \frac{50}{L_s^4} \int_{-1}^{1}\int_{-1}^{1} u^2 v^2 \left[D_\alpha\left(\frac{L_s}{2} u\right) + D_\alpha\left(\frac{L_s}{2} v\right) \right.$$

$$\left. - D_\alpha\left(\frac{L_s}{2} u - \frac{L_s}{2} v\right) \right] du\, dv \qquad \text{(B-13)}$$

By use of $D_\phi(r) = C_\phi^{5/3} |r|^{5/3}$ we find

$$D_{\gamma_2}\left(\frac{L_s}{2} x - \frac{L_s}{2} y\right) = D_{\gamma_1}\left(\frac{L_s}{2} x - \frac{L_s}{2} y\right)$$

$$+ K_\phi^{5/3} \left\{ - \frac{5}{3} (x^2-y^2) \left[x^{5/3} - y^{5/3} \right] \right.$$

$$- \frac{5}{2} (x^2-y^2) \int_{-1}^{1} z^2 \left[(z-y)^{5/3} - (z-x)^{5/3} \right] dz$$

$$\left. + \frac{25}{8} (x^2-y^2)^2 \int_{-1}^{1}\int_{-1}^{1} u^2 v^2 \left[u^{5/3} + v^{5/3} - (u-v)^{5/3} \right] du\, dv \right\} \qquad \text{(B-14)}$$

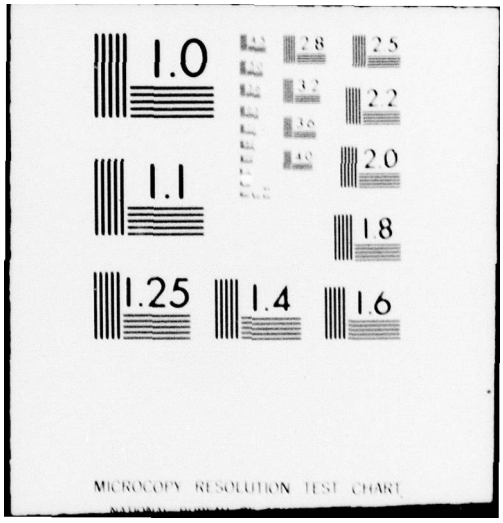
AD-A057 980 ENVIRONMENTAL RESEARCH INST OF MICHIGAN ANN ARBOR RA--ETC F/G 20/14
EFFECTS OF ATMOSPHERIC TURBULENCE ON SAR PERFORMANCE.(U)
JUN 78 G ADAMS, R CRANE, J AUTERMAN F33657-77-C-0229

UNCLASSIFIED ERIM-127800-5-F NL

2 OF 2
AD
A057 980



END
DATE
FILMED
10-78
DDC


1.0
1.1
1.25
1.4
1.6
2.8
2.5
2.2
2.0
1.8
MICROCOPY RESOLUTION TEST CHART

Both integrals can be evaluated and the average pattern with focus correction is

$$E|f(x)|^2 = L_s^2 \int_{-1}^{1}\int_{-1}^{1} A\left(\frac{L_s}{2}u\right)\overline{A}\left(\frac{L_s}{2}v\right) e^{-\frac{2\pi L_s x(u-v)}{\lambda R}}$$

$$e^{-\frac{1}{2}K_\phi^{5/3}h(u,v)}\, du\, dv \qquad \text{(B-15)}$$

where $h(u,v) = q(u,v) - \frac{5}{3}(u^2-v^2)\left[|u|^{5/3} - |v|^{5/3}\right]$

$$+ \frac{5}{2}(u^2-v^2)\left[k(u) + k(u) - k(v) - k(-v)\right]$$

$$+ 0.32\,(u^2-v^2)^2 \qquad \text{(B-16)}$$

$$k(x) = (1+x)^{8/3}\,\frac{27x^2 - 72x + 132}{616} \qquad \text{(B-17)}$$

To write $E|f(x)|^2$ when A = 1 in normalized form requires

$$E|f(x)|^2 = L_s^2\, g_2\left(\frac{2L_s x}{\lambda R}\,;\, K_\phi\right) \qquad \text{(B-18)}$$

where $g_2(x;\, K_\phi) = \frac{1}{4}\int_{-1}^{1}\int_{-1}^{1} e^{-j\pi x(u-v)}\, e^{-\frac{1}{2}K_\phi^{5/3}h(u,v)}\, du\, dv \qquad \text{(B-19)}$

Figures 8 and 9 show $g_2(x;\, K_\phi)$ for x between 0 and 6 and varying values of y.

REFERENCES

1. V.I. Tatarski, Wave Propagation in a Turbulent Medium, Dover Publications, Inc., New York, 1961.

2. M.C. Thompson, Jr., H.B. Janes, L.E. Wood, and D. Smith, Phase and Amplitude Scintillations at 916 GHz on an Elevated Path, IEEE Trans. AP, November 1975.

3. L.J. Porcello, Turbulence-Induced Phase Errors in Synthetic Aperture Radars, IEEE Trans., AES, September 1970.

4. M.C. Thompson, Jr. and H.B. Janes, Measurements of Phase-Front Distortion on an Elevated Line-of-Sight Path, IEEE Trans., AES, September 1970.

5. W.M. Brown and J.F. Riordan, Resolution Limits with Propagation Phase Errors, IEEE Trans., AES, September 1970.

6. M.C. Thompson, Jr., F.E. Marler, and K.C. Allen, Measurement of Refractive Index Parameters for Calculating Limits of SAR Image Resolution, OT Technical Memorandum 77-233, U.S. Department of Commerce/Office of Telecommunications, Boulder, Colorado, April 1977.

7. J.W. Strohbein, Covariance Functions and Spectra for Waves Propagating in a Turbulent Medium to or From Moving Vehicles, IEEE Trans., AP, March 1975.

8. D.W. Curtis, Atmospheric Induced Phase Error Effects in Synthetic Aperture Radar Systems, A EEM No. 458, Goodyear Aerospace Corporation, Arizona Division, Litchfield Park, Arizona, July 1973.

9. M.J. Vetter and M.C. Thompson, Jr., Solid-State Microwave Refractometer, Rev. Sci. Instrum., Vol. 38, No. 12, pp. 1726-1727, 1967.